Humanization of Chimeric Antigen Receptors (CARs) OSCAR-1 and OSCAR-3

Molecular biology and biochemistry (2023)

60 ect

By Pia Ahnstrøm

Acknowledgements

Firstly, I would like to thank Sébastien Wälchli and Else Marit Inderberg for accepting me into their laboratory and giving me the opportunity to work on this project, as well as providing me with the facilities and resources necessary to complete my thesis.

To Nadia Mensali and Sandy Joaquina, I sincerely thank you for your hard work on OSCAR-1 and OSCAR-3, without this my thesis as it stands would not exist. Your patience, and illuminating answers to my many questions regarding the OSCARs could not have been better provided by anyone else.

To Christopher Forcados, I give my earnest appreciation for the countless hours of patience, support and drive. Your guidance through practical and theoretical learning has been essential for my academic development throughout this project, and your persistance has been contagious.

Finally, I would like to express my gratitude for all my supportive colleagues at Cell Therapy, Translational Research Unit, Radiumhospitalet, your positive attitudes and shared excitement for this project has been invaluable in stressful periods. The many shared coffee breaks and laughs have provided me with motivation through challenging times. To Klara Krpina, your unwavering supportive words have been crucial, and to Wafa Kefi, your presence and positive outlook have made our shared office an inspirational place to work.

Table of content

1. Introduction

1.1 Osteosarcoma

Osteosarcoma (OS), a malignant tumor of the bone, is one of the most common forms of cancer among adolescence, presenting in more than 5 per 1 million children under 15 years of age. The occurrence of OS has a bimodal distribtion across age groups: While the incidence peak worldwide is around pubertal growth spurt, the occurrence rate increases again around the age of 60 years. Generally, men are more affected than women, and this trend is even more prominent in the elderly[1]. The occurrence of OS is uneven among ethnic groups, with blacks and hispanics being overrepresented, and the cause of this is unknown[2]. Globally, the occurrence of OS is quite evenly spread across continents in the adolescent age group, but in the elderly the prevalence increases in the United Kingdom, Australia and Canada, compared to the rest of the world[3].

OS originates from mesenchymal cells and is most commonly found in the long bones, particularly in the distal femur and the proximal tibia or humerus. While primary tumors usually form in the metaphysis of long bones, secondary tumors have a wider distribution throughout the body, with an elevated incidence rate in the pelvis. With primary OS, the most common site of metastatic disease is the lungs, followed by the bowels, the heart and the brain[4]. The disease is histologically quite diverse, and can roughly be divided into various subtypes depending on the grade, and the location of the lesion within the bone. High grade and low grade OS refers to the morphology of the cancerous cells in comparison to healthy cells, and has some prognostic value; low grade tumor cells refer to a low grade of nuclear atypia, and is associated with better prognosis. Within the affected bone, the lesion may be central, located in the medulla, or periosteal/cortical, located on the surface of the bone, or extraskeletal, located in the softer connective tissues[5].

Before the 1970s, the standard of care for OS was amputation, and only 20% of patients survived for more than 5 years. With the introduction of post-surgical chemotherapy in the 80´s, survival rates increased to 61% for 6 year survival, and it´s use complementary to surgery became standardized[6]. The last quarter of the 1900s saw different combinations of chemotherapeutical agents being used, with great controversy surrounding the question of what the optimal regimen was, due to conflicting evidence caused by nonrandomized studies. However, international group

efforts later determined that the most effective chemotherapeutical cocktail for OS patients consisted of high-dose methotrexate, cisplatin and doxorubicin, which has remained the gold standard since then[7]. Unfortunately, the long-term survival rate for patients with metastatic disease remains dismal, with only 20-40% of patients seeing survival past 5 years[8]. Chemotherapeutical agents do not discriminate their effects between normal and abnormal cells, and while successful at eradicating cancer cells, a large number of healthy cells are also killed during chemotherapy. Long term side effects include heart attacks and cardiovascular disease, cytopenia, hearing loss, and gonadal toxicity[9], and the need for new therapies with improved success rate and less side effects is urgent.

In *in vitro* and pre-clinical models, the therapeutic use of Programmed cell death protein-1 (PD-1) inhibitors showed promising results against OS[10], however a phase II clinical trial treating patients with unresecteable, relapsed OS with the antibody Pembrolizumab reported no significant anti-tumor effect after 4 and a half months of treatment[11]. Tragically, 11 patients had succumbed to OS before this trial was terminated. Three other clinical trials examining the anti-tumor activity of immune checkpoint inhibitors (ICI), namely Ipilumab and Nivolumab (both anti-PD-1) and Atezolizumab (anti-PD-Ligand 1 (PD-L1)), against OS also showed no significant clinical benefit[12]. Summarized, evidence gathered so far indicates that monotherapeutical regimens with ICI or chemotherapeutical agents against OS are unsuccessfull. Recently, research into Chimeric Antien Receptor (CAR) T cells as treatment against OS has progressed to multiple clinical trials, targeting several different antigens. Among the antigens targeted by CAR T cells in these clinical trials are human epidermal growth factor receptor-2 (HER-2) (NCT04995003), epidermal growth factor receptor (EGFR) (NCT03618381), the disialoganglioside GD2 (NCT04539366), and the B7 homolog 3 protein (B7-H3) (NCT04897321). So far, HER-2 CAR T cells have been deemed safe for use and well tolerated as therapy against a variety of sarcomas in a phase I clinical trial, but results regarding the tumor controll are not yet available. Results from the clinical trials targeting GD2, EGFR and B7-H3 are not yet available.

Due to the fact that most patients of malignant bone tumor are children and teenagers in a critical and sensitive developmental period of life, the quality of life after therapy should be specially considered. Treatment should aim to be as minimally invasive as possible, to preserve physical

functions required in a normal everyday life of adolescents. Limb salvation surgery (LSS) has been showed to be equally as effective as limb amputation in the context of post-operative local recurrence, and patients who receive LSS have a significantly higher 5 year survival rate compared to patients undergoing amputation[13]. The implementation of allograft bone reconstruction or metallic prosthetics after distal femur or proximal tibia resection has improved the quality of life for adolescents and young adults with sarcoma in lower extremities substantially, even allowing patients to return to high-impact sports[14].

Research into the causes of OS has uncovered that while most of the cases are sporadic, there are genetic predispositions responsible for a small percentage of cases. The hereditary cancer syndromes Retinoblastoma (Rb), Li-Fraumeni syndrome, Werner syndrome and Bloom syndrome are among the disorders that can cause OS, as well as other cancer types[15]. The increased risk associated with these syndromes is caused by germline mutations in tumor suppressor genes, or oncogenic mutations in genes involved in DNA maintenance. The genes most commonly mutated in OS are the c-Myc, the Rb protein and the P53 genes. Oncogenic c-Myc promotes invasion of neighboring tissues through aberrant MEK-ERK signaling, thereby stimulating metastatic disease. Rb and P53 are both tumor suppressor genes, and the loss of their wild type function stimulates cellular transformation. Specific driver mutations have also been indentified in NOTCH1, BRCA2, and FOS genes among others, affecting cell fate determination[16], DNA damage repair and cell proliferation[17]. Certain micro RNAs (miRNAs) have also been identified as activators of aberrant MAPK and PI3K/Akt signaling, such as miR-21, -34a and -143. A characteristic molecular event of sarcomagenesis is the loss of CDK inhibitor functions, resulting in uncontrolled cell cycle progression. This loss of function may be caused by deletions in tumor suppressor genes like PTEN, or amplification of oncogenes such as CDK4 and MDM2, or a combination of these factors[18].

Tumor initiating cells (TICs), also called cancer stem cells, are cells capable of renewal and proliferation at such a rates that tumors are able to form from their progeny cells. The phenotype arising from the mutations accumulated in TICs highly promotes their survival in primary lesion sites, as well as at distant pre-metastatic sites. Their presence is associated with drug resistance, metastatic growth and relapse. The cell surface marker CD133 has been highlighted as a potential marker for TICs in OS, and has been identified in four OS cell lines widely used in

research; Saos2, MG63, U2OS[18] and OSA[19]. CD133+ cells exhibit stem cell like gene expression, and cells isolated from CD133+ OS spheroids have been demonstrated to generate large tumors *in vivo*[20]. These features highlights CD133 as a potentiall target for future therapies against OS.

1.2 Immune system

The immune system is the body's defense against an array of foreign and pathological particles and microbes, and is comprised of the innate and the adaptive immune systems (illustration 1). The innate immune system is the first line of defense and consists of physical barriers, such as skin and mucous membranes, as well as non-specific immune cells and proteins, and is present from birth. The innate immune response is rapid and takes effect only minutes or hours after the initial aggression. It is comprised of multiple types of cells and molecules, like macrophages, neutrophils, dendritic cells and complement proteins, who recognize conserved features associated with many pathogens through pattern recognition receptors (PRRs). Conversely, the adaptive immune system is continually developing as one is exposed to different antigens throughout life, and is composed of the humoral branch, mediated by B cells, and the cellular branch mediated by T cells. Adaptive immunity requires several days to mount a significant response against antigens, and provides immunological memory resulting in a rapid and amplified response upon re-exposure to the antigen. Immunological memory is provided by subpopulations of the activated B- or T cells called memory cells, who will continue to circulate in the body for years after the first exposure[21].

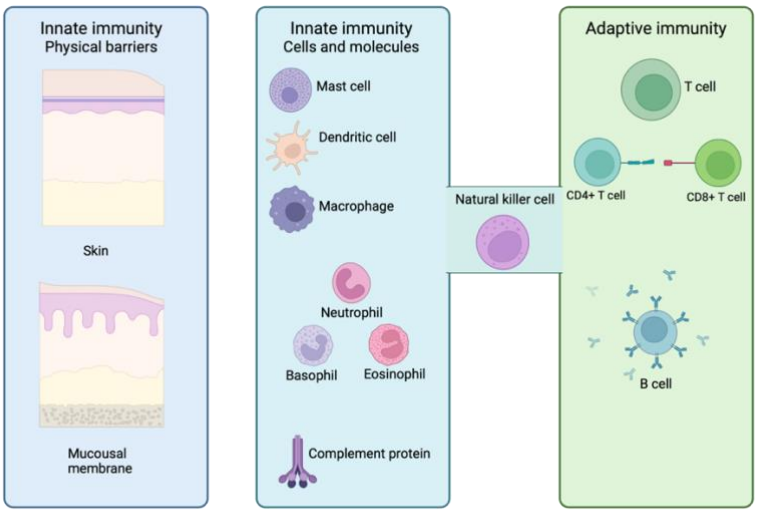

Illustration 1: Main players of innate and adaptive immunity. The figure illustrates the physical barriers, cell types and molecular componens of the innate and adaptive immune systems. Made in Biorender by Pia Ahnstrøm (PA).

1.3 The immune system and cancer development

Our understanding of the complex relationship between tumor cells and immune cells in tumorigenesis is improving, while simultaneously opening new doors into the research field of personalized medicine. Dunn *et al.* hypothesized in 2004 that cancer cells negatively edit immune cells' ability to recognize and destroy pre-cancerous and cancerous cells through 3 critical phases: Elimination, equilibrium and escape. Their hypothesis describes how the immune system, in efforts to eradicate abnormal cells with pathological potential, inadvertently shapes the cancer cell phenotypes, eventually resulting in their immune escape[22]. Accumulation of mutations occur both in healthy and malignant cells, and is partially caused by external factors like UV rays, chemicals and infections, and partially caused by internal factors like errors is DNA replication and repair. The location and nature of the mutation, as well as the total mutational burden of the specific gene, or genes involved in epistatic genetic regulation, are all factors that determine how detrimental the effects of the mutation will be. Mutations in genes, or sequences involved in the regulation of genes encoding proteins involved in DNA replication, cell growth, cell cycle progression and apoptosis pathways in particular, are more likely to have oncogenic effects. During the immune reaction against cancer cells in the early phases of tumorigenesis, a low number of cancer cells are able to evade immune cell destruction. This is at least partly due to the heterogeneous nature of solid tumors. Because the cancer cell genome is destabilized, advantageous, neutral and detrimental mutations accumulate faster in these cells compared to healthy cells where the DNA repair machinery is intact. The cells whose phenotype becomes increasingly fit to survive and proliferate in the specific biological milieu, may be able to generate tumors and metastases despite the immune systems efforts to eradicate them. This is due to their enhanced cellular growth and proliferative rate, caused by mutations resulting in uncontrolled cell cycle progression. While immune cells attack and destroy the cancer cells of low and mediocre fitness, they simultaneously increase the selective pressure amongst the tumor cells with the abilities to evade immune detection, invade neighboring tissue, and potentially metastasize at distant sites. This effectively shapes the trajectory of the most fit cancer cells and their future lineage, stimulating the continued immune escape of the cancer cells that survive.

1.4 Liquid and solid tumor, different challenges

In the last decade, clinical trials treating patients with liquid malignancy have demonstrated astounding results with CAR T cells targeting CD19, with up to 81% of relapsed or refractory B cell Acute lymphoblastic leukemia (B-ALL) patients seeing complete remission. While toxicities, including cytokine release syndrome (CRS) and neurotoxicity (NT), have been reported in a large portion of patients, these were transient and manageable in the clinical setting[23]. Such high comparable results have not yet been demonstrated in solid tumors, due to a number of challenges such as tumor heterogeneity, immunosuppressive tumor microenvironment (TME), and poor tumor infiltration. A phase I-II clinical trial investigating the tumor-controll of an anti-disialoganglioside (GD2) CAR T cells against relapsed/refractory high-risk neuroblastoma was published in 2023, where only 33% of patients saw complete response 6 weeks post infusion[24].

In regards to malignancies of B cell origin, both healthy and abnormal cells express the cell surface marker CD19. The strategic targeting of CD19+ cells results in eradication of both healthy and malignant B cells, which while suboptimal, is manageable in clinical settings. CD19+ cancer cells are readily accessible in the blood stream. Conversely, in solid tumor, the TME poses several challenges not present in liquid malignancy including hypoxia, increased interstitial pressure, low nutrient density, and acidic milieu. Solid tumors are surrounded by extracellular matrices and stromal cells, presenting physical barriers against T cell entry, as well as chemokine and cytokine compositions discouraging the homing of cytotoxic T cells to cancerous lesions (illustration 2). While cytotoxic T cells are inhibited from localizing to solid tumor, immune suppressor T cells and myeloid-derived suppressor cells (MDSCs) are attracted to the TME chemokine composition, and effectively inhibit tumor surveillance and anti-tumor activity further[25].

The vasculature surrounding tumors are characterized by irregular organization, uneven diameter and abnormal bulging, all factors contributing to low oxygen and nutrient density, as well as elevated levels of metabolic waste products[26].

Elucidating strategies to circumvent these challenges of T cell tumor infiltration is a current area of research, particularly in the setting of Adoptive cell therapy (ACT). The addition of

chemokine receptors complementary to the chemokine profiles secreted by solid tumors to CAR T cells, encouraging tumor-specific localisation, is one such strategy[27].

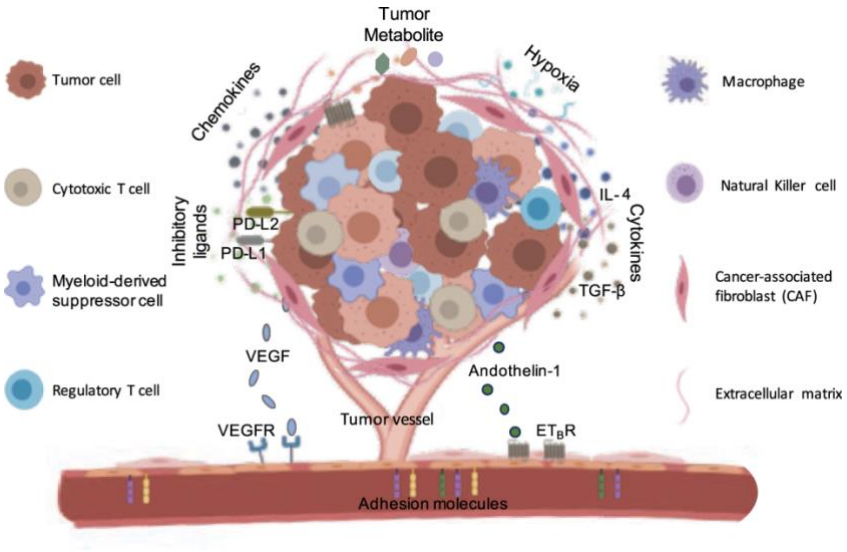

Illustration 2: Solid tumor microenvironment. The figure illustrates factors of the solid TME, and the challenges they present in the context of cell therapy[25].

1.5 T cells

T cells are primary lymphocytes derived from the common lymphoid progenitor cell which, once matured and activated, mediate cytotoxic activity against specific target cells. Lymphoid progenitor cells migrate from bone marrow to the thymus where they develop into naïve T cells. In the thymus, $CD4^+CD8^+$ double positive thymocytes´ T cell receptors (TCRs) interact with specialized cells expressing an array of different self-peptides bound to Major histocompatibility complex (MHC) class I or II molecules. As the thymocytes´ CD8 co-receptor interacts with MHC I molecules, and the CD4 co-receptor interacts with MHC II, the double positive cells are inducible by proximal cells expressing either MHC molecule. Through negative selection, thymocytes with TCRs that bind the self-peptide-MHC complex too strong, or not at all, is eliminated. A T cell with high affinity for self-peptides in the context of MHC molecules is prone to attack host cells, while a T cell that doesn't recognize either MHC I or MHC II molecules is effectively useless, because the TCR is capable of recognizing antigens only through the peptide-MHC (pMHC) complex. Cells that bind self-peptide-MHC complexes with an appropriate affinity progress through positive selection, after which the expression of either co-receptor CD4 or CD8 is silenced, resulting in single positive $CD4^+$/$CD8^+$ naïve T cells[21]. In peripheral lymphoid organs, naïve T cells must be activated in order to differentiate into $CD4^+$ helper cell (T_H) or $CD8^+$ cytotoxic cell (T_C) phenotypes, and proliferate to the extent that they may efficiently eradicate pathologies and infections. T cells are activated by Antigen presenting cells (APCs), mainly activated dendritic cells, which present foreign peptides in the groove of MHC molecules to the TCR, as well as provide a co-stimulatory ligand for the T cell extracellular CD28. The peptides in the MHC groove may be derived from intracellular proteins or membrane bound proteins from the specific target cell. Without co-stimulation of CD28, the T cell will be anergic, and both effector functions and proliferation may be inhibited.

Upon TCR engagement by a compatible pMHC, an intracellular signaling cascade resulting in activation of specific cellular responses is triggered. The Lymphocyte-specific protein tyrosine kinase (Lck)[28] is recruited to the TCR complex (illustration 3) and phosphorylates Immunoreceptor tyrosine-based activation motifs (ITAMs) located on the intracellular signal-mediating CD3ζ,, creating binding sites for the Zeta-chain-associated protein kinase 70 (Zap70).

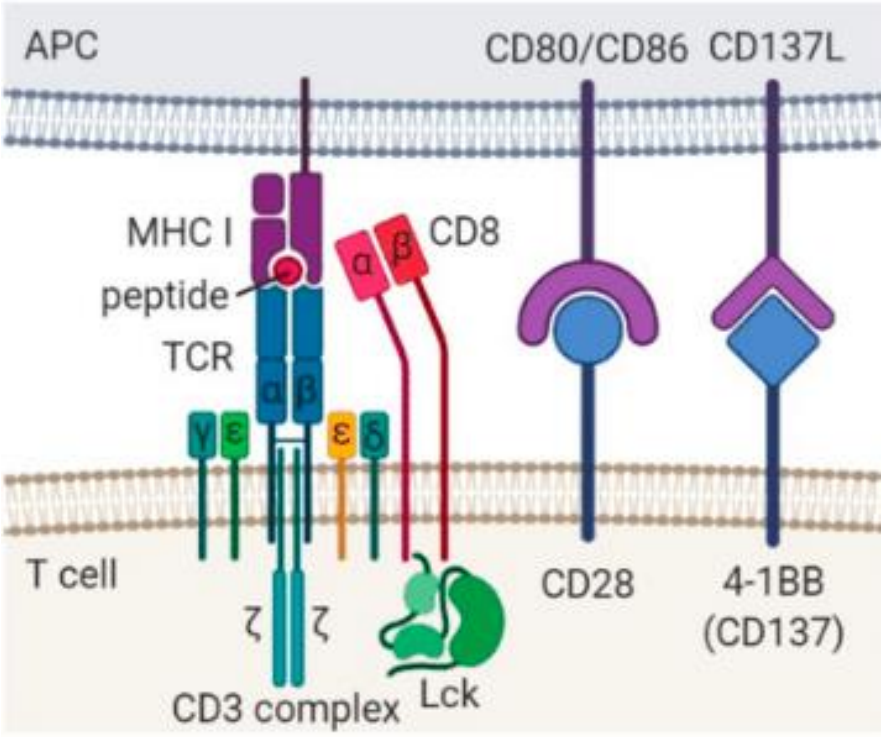

Illustration 3. TCR, CD28 and 4-1BB activation. The modified illustration shows the TCR and CD8 interacting with pMHC I, and costimulatory receptors CD28 and 4-1BB interacting with their cognate ligands CD80/CD86 and CD137L, respectively[29].

Zap70 subsequently phosporylates the Linker for activation of T cells (LAT), which in its activated stated is able to recruit a number of different signaling molecules, determined by the position of the tyrosine residue Zap70 phosphorylated. In unison, the TCR and costimulatory CD28 molecules activate phosphoinositide 3-kinase (Pi3k), which through a series of reactions result in the formation of IP_3, who´s cognate ligand is the IP3 Receptor (IP3R) located in the Endoplasmatic Reticulum (ER). Binding of IP3 to IP3R results in an influx of ca^{2+} to the cytoplasm, leading to the activation of Calcineurin, which in turn dephosphorylates cytoplasmic Nuclear factor of activated T cells (NFAT)[30]. Dephosphorylated NFAT translocates to the nucleus, where it induces expression of genes involved in T cell activity by binding to the NFAT repsonsive promoter. Additionally, TCR and CD28 activation induces expression of genes under the control of promoters responsive to the transcription factors (TFs) Nuclear factor kappa B (NF-κB) and Activator protein-1 (AP-1) (illustration 4).

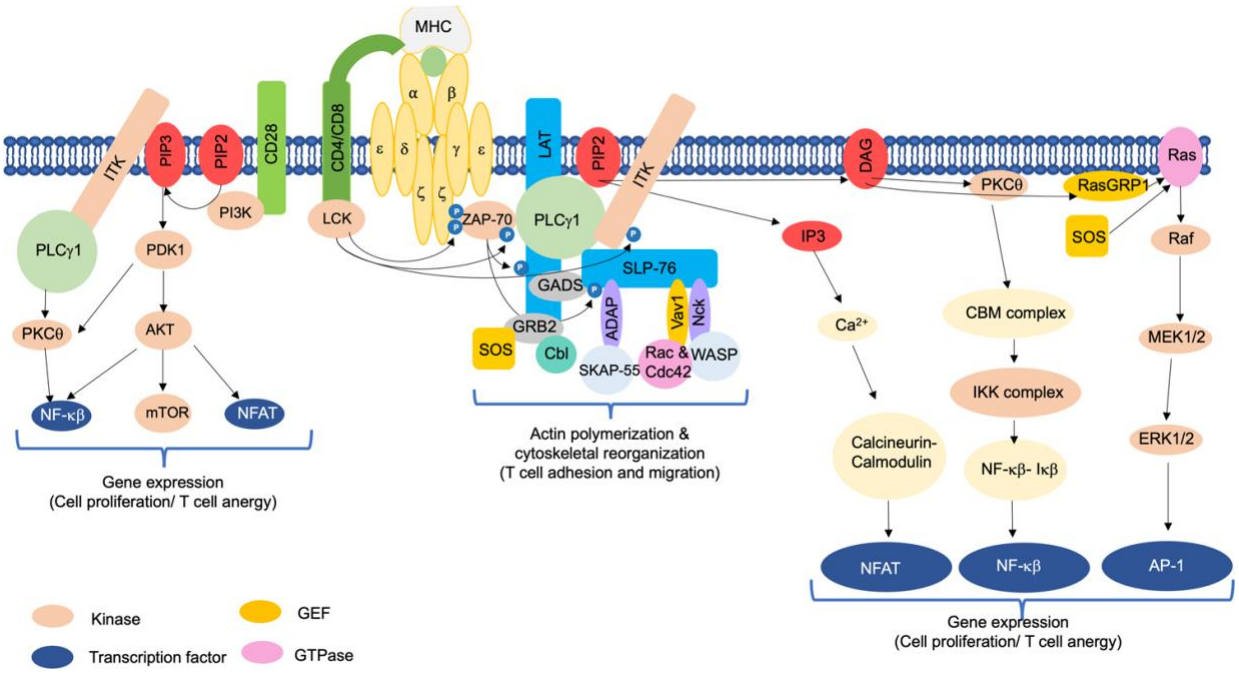

Illustration 4[31]. T cell activation signalling pathway. The illustration shows the intracellular signalling pathway from TCR and CD28 activation, to activation of transcription facors AP-1, NF-κB and NFAT.

1.6 Immunotherapy

In the past few decades, the role of the immune system in cancer development has been thoroughly investigated. Immunotherapy against cancer is the therapeutic strategy involving manipulation or genetic editing of autologous immune cells, to enhance their anti-cancer functions or redirect their specificity towards tumor associated antigens (TAA), or ideally tumor specific antigens (TSA). Established immunotherapeutic strategies include, but are not limited to, adoptive cell transfer and immune checkpoint inhibition.

Adoptive Cell Transfer

Since the late 1980s, adoptive cellular transfer has emerged as an attractive alternative or complementary therapeutic strategy to traditional cancer therapies, like chemotherapy and radiation[32]. ACT is a therapeutic strategy that utilizes the patient's autologous lymphocytes by isolating them from blood, genetically modifying the T cells with either TCRs or CARs specific for tumor antigens, followed by *ex vivo* expansion and infusion of the modified T cells back into the patient. Tumor-infiltrating lymphocytes (TILs) specifically may also be isolated from the cancer bearing host, expanded *ex vivo* and infused back into the patient to combat tumor growth. TILs are lymphocytes isolated from tumor, who naturally developed the ability to infiltrate the specific solid tumor. Unfortunately, TILs are composed of T cells with different specificities, and only a fraction of them are tumor reactive[33]. ACT utilizing modified TCRs only recognizes tumor antigens in the context of MHC molecules, and it is well known that many cancer types down regulate MHC expression in order to evade the immune system[34]. This method of immune evasion renders TCR T cells blind to MHC^- cancer cells. The MHC dependence of TCRs pose critical limitations in the perspective of cell therapy. The idea of circumventing this limitations, and inducing the cytotoxic effector functions of T cells through alternative means was the basis for the development of synthetic CARs, who function independently of MHC molecules. Additionally, the antigen binding domains of CARs are of antibody origin, resulting in higher antigen affinity compared to TCRs, who are eliminated through negative selection as described previously. TCRs are membrane-bound, heterodimeric proteins that most commonly consist of one α- and one β- chain linked together by disulfide bonds. Each chain is comprised of one variable (V) domain, containing three complementarity-determining regions (CDRs), and one constant (C) domain with conserved cysteine residues that link the α- and β- chain together. The

TCR is attached to an intracellular CD3ζ molecule, that is required for signal transduction through ITAMs. CARs, by comparison, are synthetic receptors able to initiate the same T cell effector functions as TCRs, independently of the target cells MHC expression profile. Additionally, target sequences do not have to fit in the peptide binding groove of the MHC molecule, allowing for targeting of immunogenic carbohydrates and glycolipids as well, enriching the potential target repertoire. Certain post ranslational modification (PTM) motifs, for example acetylation or glycosylation of specific amino acids, are associated with tumor cells. The addition of these motifs alters the function of the protein, potentially increasing their oncogenic effect, but may also induce stronger immunogenicity[35]. Proteins with cancer associated PTMs may therefore be potential targets for CAR therapy. The development and optimization of CARs has been a research area of great interest due to the vast potential these synthetic receptors present with, and has led to the design of several types of CARs (illustration 5). The first generation of CARs existed simply of the extracellular antigen-binding single chain Fragment variable (scFv), a hinge and transmembrane domain, and the intracellular CD3ζ domain mediating downstream signaling through the same mechanism as in TCRs. The transmembrane domain anchors the receptor to the plasma membrane, while the hinge provides additional mobility to allow the scFv to interact with target antigens distal or proximal to the cell membrane. Further development of these receptors included the addition of one or more co-stimulatory domains, in order to improve activation and enhance the CAR T cells persistence and durable cytokine release. Currently, T cells redirected for universal cytokine-mediated killing (TRUCKs) armed with inducible or constitutively expressed chemokines, and next-generation CARs with additional cytokine receptor binding motifs, are being developed to mediate synergistic signaling profiles and improve T cell tumor infiltration, proliferation and survival[23].

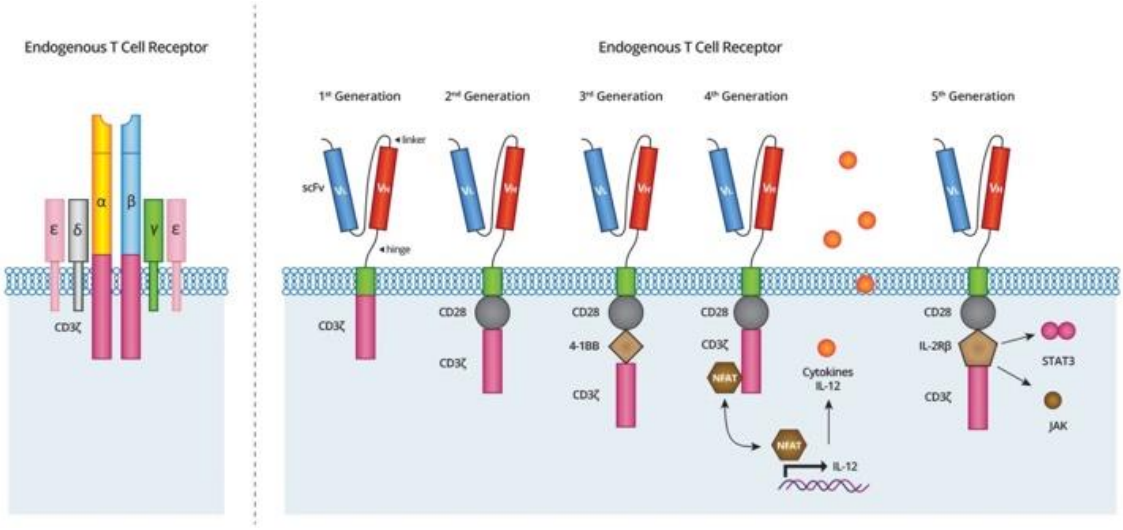

Illustration 5: TCR and CAR designs.The figure illustrates the molecular differences between TCRs and different generation CARs[36].

Immune checkpoint inhibition

Immune checkpoints are molecular parts of a well-functioning immune system, responsible for suppressing immune reactions to limit the damage of healthy host cells during the attack of a foreign substance. Their function is essential for maintaining self-tolerance and preventing autoimmunity, but also taken advantage of in tumorigenesis. On the surface of T cells, receptors which induce negative regulation of T cell activation are expressed, such as PD-1 and Cytotoxic T-lymphocyte-associated protein 4 (CTLA-4) (illustration 6). When the PD-1 receptor bind its cognate ligand PD-L1, suppression of T cell activation pathways are induced[37]. The signaling pathways downstream of the PD-1 receptor leading to inhibition of T cell avtivation are not very well understood yet.

In a similar effect, activation of the CTLA-4 receptor via its cognate ligand, CD80 and CD86, induces phosphatases which subsequently dephosphorylate signaling molecules involved in T cell activation. This interaction actively inhibits T cell activation upon TCR-peptide-MHC and co-stimulatory CD28-B7 interactions[38]. The upregulation of the PD-1 and CTLA-4 receptor ligands is a strategy cancer cells employ to down regulate the cytotoxic functions of proximal T cells.

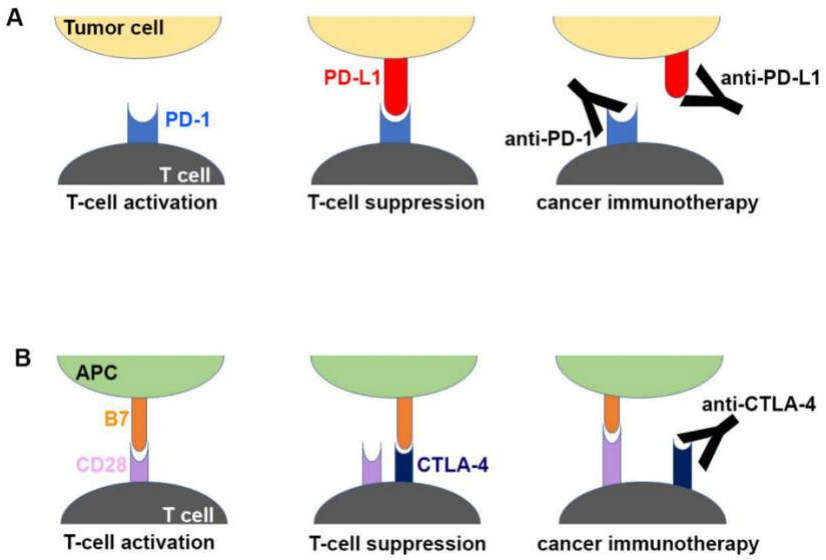

Illustration 6: T cell inactivation by tumor and re-activatiton by ICI. The figure illustrates the mechanism of action behind cancer cell inactivation of T cells, and how therapeutic antibodies target this suppressive interaction to re-initiate T cell cytotoxicity[39].

The therapeutic use of monoclonal antibodies (mAbs) targeting receptor-ligand interactions responsible for the suppression of T cell effector functions is an area of active research. In 2018, James P. Allison [40] and Tasuku Honjo[41] were awarded the Nobel Prize in physiology or Medicine for their work elucidating the roles of Immune checkpoint proteins, and how they may be manipulated in cancer therapy (illustration 6).

The clinical application of ICI have revolutionized the landscape of cancer therapies, demonstrating increases in long term tumor controll from 10% to almost 50% of patients with advanced melanoma[42] . However, many patients still show resistance to single-agent ICI, and combinatorial regimens are currently being investigated[43].

1.7 OSCAR

In 1986 researchers at Radiumhospitalet in Oslo, Norway, isolated two mAbs from mice inoculated with human OS, named TP-1 and TP-3. They were demonstrated to recognize and bind 15/15 OSs tested, 3/3 synovial sarcomas tested and several other types of sarcoma. Additionally, these murine antibodies were not cross-reactive against non-sarcomatous cancer cells or peripheral blood lymphocytes[44].

Recently, our group identified the target epitope of TP-1 and TP-3, and discovered that it is a specific isoform of an alkaline phosphatase, namely ALPL-1, strongly associated with OS and found to be expressed at the cell surface of 90% of OS metastases. While alkaline phosphatases are normally expressed in a variety of healthy tissues, the specific isoform targeted by TP-1 and TP-3 was identified only in OS cells and proliferating osteoblasts. The target sequences were subsequently subcloned into second generations CARs, consisting of the intracellular CD3ζ signalling domain, a 4-1BB co-stimulatory molecule, a CD8 transmembrane domain and hinge, and the extracellular scFv antigen binding domain derived from TP-1 and TP-3. These CARs targeting OS were named OSCAR-1 and OSCAR-3, and functionally tested both *in vitro* and *in vivo*. The cytotoxic activity against target positive cell lines was comparable between OSCAR-1 and -3, but the cytokine release profile showed differences between the two constructs, indicating a higher potency in OSCAR-3. In human OS (hOS) xenograft models with lung metastases, both OSCARs demonstrated efficient control of metastatic diseases and prolonged survival[45] (illustration 7).

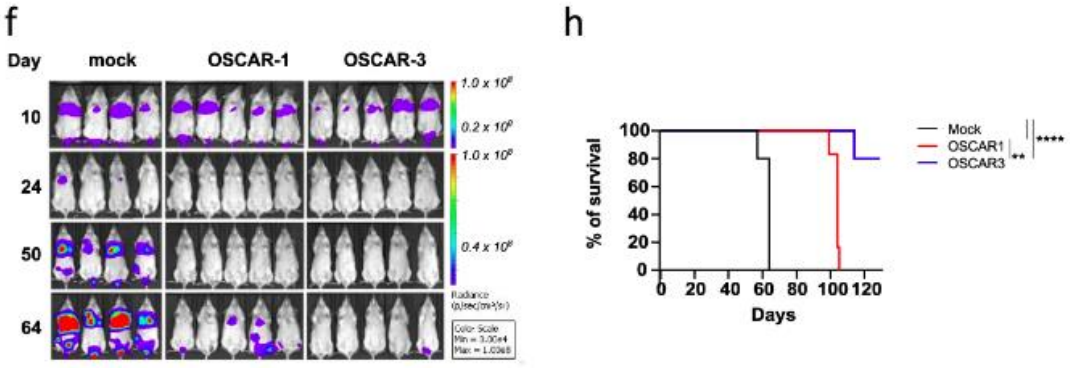

Illustration 7: Tumor controll by OSCAR-1 and -3 in hOS xenograft model. The modified illustration shows controll of metastatic hOS disease by OSCAR-1 and -3 in xenograft model[45].

1.8 Humanization

The use of genetic sequences of non-human origin is common in the context of CAR design[46], both in the heavy and light chain of the scfv, and in process of producing CARs. Transduction of the genetic CAR sequence is often mediated by γ-retroviral or lentiviral vectors. With the use of retroviruses in genetic therapy, risk of insertional mutagenesis is present. Insertion of the viral vector into the host genome is semi random, and may trigger cellular transformation if inserted near oncogenes. This risk can be minimized with the use of retroviral vectors with sequence preferences; γ-retroviruses for example, insert in clusters near sequences with motifs like CpG islands, and trascriptional start sites[47]. While several CARs utilizing antigen binding domains of murine origin have been deemed safe and approved for treatment of a variety of cancers, both humoral and cellular immune responses have been observed in patients treated with this type of CAR. Human anti-mouse IgG antibodies have been found in the blood of patients receiving CAR T cell therapy, but this event has generally been considered harmless in the context of adverse events[48]. Strong immune reactions however, can lead to CAR T cell depletion, lowering the anti-tumor effects and increasing likelihood of relapse[49], as well as life threatening anaphylactic reactions. In one clinical study with repeated infusions of anti-mesothelin CAR T cells, one out of four patients developed acute anaphylaxis after the third infusion, leading to cardiac arrest. The authors of this study conclude that this adverse event was caused by induction of IgE antibodies specific for the murine-based antibody sequence from which the antigen-binding domain of the CAR was derived. They importantly note that while the occurrence of anaphylaxis in this specific clinical setting was high, from their history with over 400 patients receiving infusion of T cells, this is the first instance of anaphylaxis[48]. While anaphylaxis is a rare adverse event, the acute life threatening nature of this condition warrants research and development of CAR design strategies to minimize the risk of anti-mouse immunogenicity. Modifying the modules on the CAR of non-human origin is one strategy to reduce the immunogenicity of CAR therapies. The scFv makes up the extracellular antigen-binding domain, consisting of one heavy chain and one light chain derived from antibody. The heavy and light chains are connected by a linker peptide. Both the heavy and light chain consist of 4 framework regions (FRs) and 3 CDRs (illustration 8). The FRs are involved in folding of the protein, arranging the antigen binding domain in such a way that it can interact with its cognate epitope. The genetic sequence encoding the FR of the scFv may be replaced with human consesus sequences, in order to reduce

immunogenicity. In order to maintain the epitope affinity and avidity, the CDRs should not be altered. This method of humanization is called CDR grafting[50].

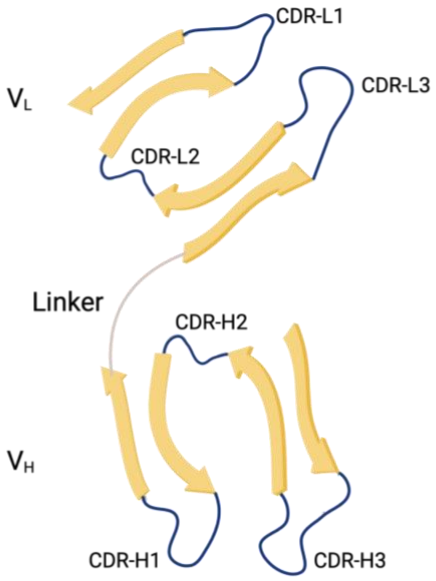

Illustration 8: The basic structure of a scFv. The illustration depicts an scFv example structure, CDRs in blue loops, linker peptide in brown, and FRs in yellow arrows. Made in Biorender by PA.

Myers *et al*. reported in 2021 the patient outcomes from a clinical trial investigating the response to a humanized CD19 CAR in young patients with relapsed or refractory B-ALL or BLL, comparing patient groups either naïve or pre-exposed to CAR T cell therapy. This study elucidated the efficacy of humanized CAR (hCAR) T cell therapy in patients after failure of prior non-humanized CAR T cell therapy, which is particularly challenging to treat. After 30 days, the overall response rate in the CAR naïve and CAR pre-exposed cohorts was 98% and 64%, respectively. Twentyfour months post-infusion, 74% of CAR naïve patients showed relapse free survival, compared to 58% of CAR pre-exposed patients[51]. These results highlight the expanded potential of hCAR T cells compared to fully murine CAR T cells, as previous studies

investigating the efficacy of re-infusion of murine CAR (mCAR) T cells has reported response rates of only 39%[52].

In 2022, Huang *et al.* compared the therapeutic effects between humanized and fully murine CD19/CD22 CAR T cell cocktail therapies in patients with refractory or relapsed aggressive B-cell lymphoma. The two patient groups received CAR T cell cocktails where the distinguishable factor was the nature of the scFv; the antigen-binding domains were either humanized or fully murine. At 3 months post-infusion, 75% of the patients treated with hCAR cocktails saw complete responses, while only 35.7% of patients receiving mCAR cocktails had equally successful outcomes[53]. Additionally, both the incidence rate and severity of reported Immune effector cell-associated neurotoxicity syndrome (ICANS) were higher in the patient group receiving murine agents.

In a Podoplanin (PDPN) -expressing solid tumor xenograft model, Ishikawa *et al.* compared the anti-tumor activity of a humanized and murine CAR targeting PDPN, a glysosylated transmembrane protein found to be highly expressed in solid tumors. The non-humanized CAR contained a scFv of murine origin, specifically a rat anti-human PDPN antibody. They reported a stabilization of the hCAR expression at the plasma membrane of T cells, as well as enhanced anti-tumor activity when compared to the non-humanized anti-PDPN CAR. Specifically, the hCAR controlled tumor growth for 35 days post T cell injection, while the mCAR only controlled tumor growth for 21 days in this *in vivo* model. They speculate that the improved anti-tumor activity of the hCAR may be partially due to PTMs affecting protein stability and function, as there was no significant difference in the mRNA transcript level of the different CARs, nor the level of total protein expression[54].

The promising results of these recent studies comparing humanized and non humanized CARs indicate that several functional features may be improved with humanization. Not only may humanization increase the CAR T cell safety profile, it may also improve the persistence and anti-tumor effects of the agent, as well as provide an additional therapeutic strategy for patients who fail to respond to, or relapse after treatment with mCARs.

1.9 Aim of this study

The aim of this study is to compare the novel humanized constructs derived from OSCAR-1 and OSCAR-3, to their murine counterpart. Specifically, to determine if humanization led to decreased recognition of murine Fragment antibody (mFab), to compare level of activation in co-culture with target positive cell line, and to compare expansion, cytotoxicity and cytokine release profiles *in vitro*, as well as *in vitro* functional persistance.

These aims will be achieved by comparing the murine and humanized scFvs:

- scFv´s staining efficiency

- CAR potency in reporter assay

- Cytotoxicity in CAR T cells

- Cytokine production in CAR T cells

- Exhaustion assay

2. Method and material

2.1 Cell lines, media and reagents

The OS cell line OSA was obtained from the American Type Culture Collection (ATCC). The human metastatic osteosarcoma cell line LM-7 was a kind gift from Dr. Eugenie Kleinerman (The University of Texas MD Anderson Cancer Center, Houston, Texas, USA).The TCR^- Jurkat (J76) cell line derivative was a kind gift from Dr. Miriam Hemskeerk (Leiden University Medical Center, Netherland). The J76 cell line was transduced with a vector encoding the green fluorescent protein (GFP) gene under regulation of an NFAT responsive promoter. A clonal polulation named E2, was isolated from the bulk population and used in NFAT reporter assays. The cell lines OSA, LM-7 and J76 were maintained in RPMI 1640 (Thermo Fisher Scientific), supplemented with 10% Fetal Bovine Serum (FBS) (Thermo Fisher Scientific) and 0.05 mg/ml gentamycin (Thermo Fisher Scientific).The Human Embryonic Kidney cell line HEK-Phoenix (HEK-P) was from our collection. The HEK-P cell line was maintained in DMEM (Sigma) supplemented with 10% HyClone Characterized Fetal Bovine Serum (Thermo Fisher Scientific) and 0.05mg/ml gentamycin. Adherent cell lines were chemically detached using Trypsin-EDTA (Sigma). Peripheral blood mononuclear cells (PBMCs) were previously isolated by density gradient centrifugation from buffy coats obtained from Oslo Blood Bank, and biobanked in liquid NO_2. T cells were grown in X-vivo 15 (Lonza) supplemented with 5% CTS Serum Replacement, and 100 U/mL Interleukin (IL)-2 (Novartis). All cells were washed with DPBS (Sigma Aldrich), and incubated at 37 °C, 5% CO_2, unless stated otherwise.

For NFAT reporter assays, Phorbol 12-myristate 13-acetate (PMA) (1:10 000) and Ionomycin (1:1000) were used to induce activation of J76E2 cells transduced with either mCAR or hCAR, or non-transduced.

Target cell lines OSA-GFP-Luc, LM-7-GFP-Luc and HEK-P-GFP-Luc transduced with a vector carrying genes for GFP and Luciferase were a part of our collection, and used for BLI assays. These modified cell lines were given the annotation GFP-Luc after cell line name. Luciferin was dispensed as a substrate to measure decline of bioluminescence produced by target cell lines as cell death increased. For Bioluminescence Imaging assays, BLI media (RPMI 1640 sans phenol

red) supplemented with 10% FBS was used to avoid interference with bioluminescence produced by target cell lines. 2% Triton was used to mimic a maximum lysis condition, to allow calculation of specific lysis.

2.2 DNA constructs

OSCAR-1 and OSCAR-3 were developed at Radiumhospitalet, Oslo. Two series of humanized OSCAR-1 and OSCAR-3 scFv's were obtained from two different biotech companies. The OS-series was produced by 1 company, and the OF-series by another. The OS- and OF-series included 4 humanized scFv's for OSCAR1 and OSCAR3 each. In total, 16 humanized scFv's were cloned into CARs and tested in J76E2 cells, and/or primary T cells.

Table 1. The table shows the construct names of the humanized scFvs.

	OS-series	OF-series
OSCAR-1	OS1-1	OF1-1
	OS1-2	OF1-2
	OS1-4	OF1-3
	OS1-5	OF1-4
OSCAR-3	OS3-1	OF3-1
	OS3-2	OF3-2
	OS3-3	OF3-3
	OS3-4	OF3-4

2.3 Cell culture

Transfection, production of retroviral particles and scFv-IgG's

HEK-P cells were cultured in 3 cm plates at concentration of $5x10^5$ cells/mL, with a total cell number of $1.5x10^6$ per plate for transfection. Transfection was performed using Xtreme-gene 9 DNA transfection reagent (Sigma), and Optimem (Life Technologies). The plasmid containing

DNA of interest (CAR) was combined with plasmids containing γ-retroviral packaging DNA (encoding gag, pol and env- genes) and a plasmid encoding the gene for GFP reporter, in a total amount of 4 µg DNA per sample (illustration 9). DNA, Xtreme-gene and Optimem were incubated at room temperature for 15 minutes before the mix was added to the HEK-P cells. Cells were then incubated over night. The following day, the transfection efficiency in the HEK-P cells was assessed by GFP-fluorescence under the microscope. Media was then changed to DMEM supplemented with 1% HyClone, and cells were incubated at 32°C, 5% CO_2, over night. The next day, supernatant was harvested and stored at 4°C, and new media was added to the cells before they were incubated at 32°C over night. The following day the supernatant was harvested again, and stored at 4°C for up to 5 days.

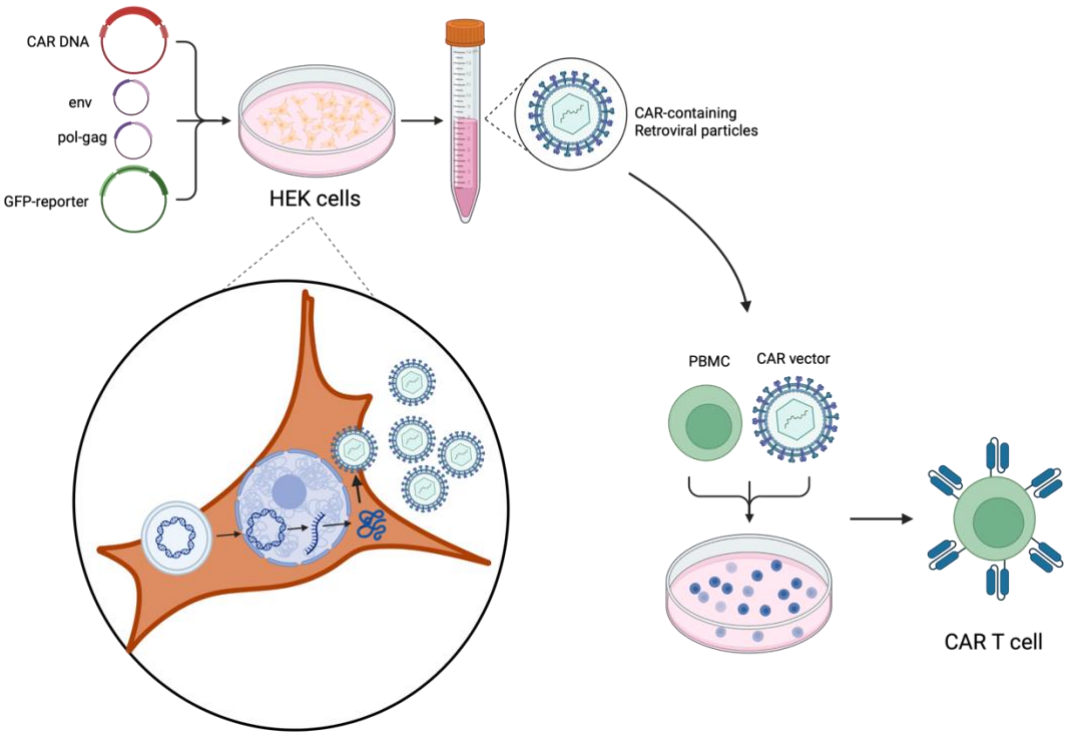

Illustration 9. Retroviral CAR-containing particle production. The illustration shows the different components and steps of γ-retroviral particle production in HEK cells. Made in Biorender by PA.

For production of scFv-IgG's, the DNA of interest was transfected into HEK-P cells with Xtreme-gene and Optimem, but without retroviral packaging DNA. The DNA, Xtreme-gene and Optimem was incubated at room temperature for 15 minutes, before the mix was added drop

wise to HEK-P cells, and incubated over night. The following day cells were assessed for GFP-fluorescence, the media was changed to IMDM 1% HyClone, and cells were incubated at 32°C, 5% CO_2, for 48 hours. Supernatant was then harvested, and stored at 4°C for up to 5 days.

In vitro retroviral transduction of J76E2 cells

A non-tissue coated 24 well plate (spinoculation plate) (Nunc multidish, Thermo Fisher) was pre-coated with retronectin (50 µg/mL) (Tanaka) for 2-3 hours at room temperature. Retronectin was removed from the wells, and replaced by 2% FBS in DPBS (after this referred to as flow buffer) for 30 minutes at room temperature for blocking. The flow buffer was removed before spinoculation. J76E2 cells were resuspended to a concentration of $0.3x10^6$ cells/mL, from which 500 µL was dispensed in each well. Five hundred µL of retroviral supernatant was added on top of this, and spinoculation was performed at 750xg, 32°C, for 60 minutes. Cells were then incubated over night. The following day the media was replaced with fresh media, and cells were incubated for an additional 24/48 hours, before CAR expression was assessed with anti-CD34t staining and Flow Cytometry.

In vitro activation, retroviral transduction and expansion of primary T cells

A cell culture treated 24 well plate (Thermo Fisher) was coated with a solution of anti-CD3 (1:1000) and anti-CD28 (1:1000) in DPBS over night at 4°C. The following day the coating solution was removed from the wells, and previously isolated and frozen PBMCs were thawed and resuspended to a concentration of $1x10^6$ cells/ mL. One mL of resuspended PBMCs was dispensed in each well, and incubated for 48h. After activation, PBMCs were collected from the 24 well plate and resuspended to a concentration of $6x10^5$ cells/mL. Five hundred µL of resuspended PBMCs were dispensed in each well of the pre-treated spinoculation plate (see *In Vitro* retroviral transduction of J76E2 cells) ($3x10^5$ cells / well), and 500 µL of retroviral supernatant was added on top. Spinoculation was performed as previously explained, and the plate was incubated over night. The following day 500 µL of media was removed from each well, and 500 µL retroviral supernatant was again added to the cells. Spinoculation was repeated, before the cells were placed back in the incubator. Day three after the first spinoculation, media was changed. The cells were kept at a concentration of $1x10^6$ cells/mL, and expanded for 11-12

days after first spinoculation. CAR expression was assessed with anti-CD34t staining and Flow Cytometry.

Cell staining

Cells were washed (centrifuged, 500xg for 5 minutes) in Flow buffer, and stained with anti-CD34-APC (1:50) antibody, and anti-mFab-Biotin (1:200) antibody and incubated for 15 minutes at room temperature. Cells were washed again in Flow buffer, before the cells were stained with the secondary antibody Streptavidin-PE (1:400), and incubated for 15 minutes in room temperature. Cells were washed, and assessed on a BD FACSCanto Flow cytometer.

2.4 Molecular biology

Cloning strategy

Our CAR constructs were designed with compatible ends (NotI-BamHI) flanking the scFv in reading frame with the rest of the CAR, followed by 2A self-cleaving peptide and a truncated CD34 (CD34t) tail (illustration 10). The 2A self-cleaving peptide and CD34t were utilized to allow for CAR detection by anti-CD34 staining. At protein level, the self-cleaving 2A would disconnect the CD34t from the CAR protein, and the CAR and the CD34t should be expressed at the cell membrane at an equimolar ratio.

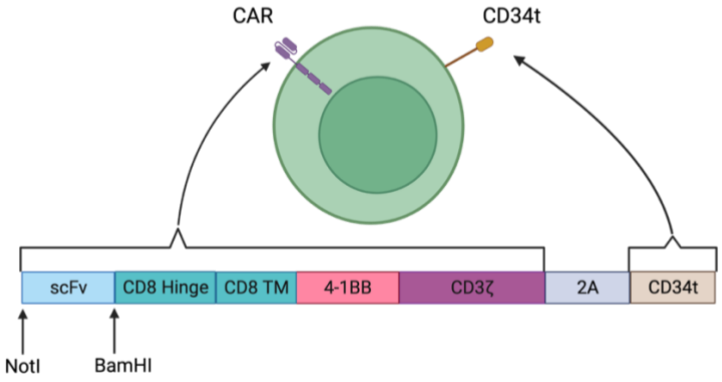

Illustration 10. Design of CAR module. The illustration shows NotI/BamHI restriction sites flanking the scFv, the CD8 hinge and TM domains followed by the 4-1BB co-stimulatory and CD3 ζsignaling domain, 2A self-cleaving peptide, and CD34t. Made in Biorender by PA.

After procuring the humanized scFv's from the biotech companies, a enzymatic digestion was performed on both the commercial vector carrying the scFv, and the vector carrying the CAR. The products of the digestion were run on a 1.5% agarose gel, and the scFv and CAR backbone (without scFv) were isolated from the gel, and extracted using a Nucleospin Gel and PCR Clean-up kit (QIAGEN). The scFv and CAR backbone were ligated using the T4 ligase, with an optimized version of the Quick Ligation Protocol (New England BioLabs). The ligation product was kanamycin resistant, and transformed into NEB5 competent *E. Coli* cells according to the High Efficiency Transformation Protocol (New England Biolabs), then plated on LB agar with kanamycin and incubated at 37° over night. The following day, 2 colonies were picked, and cells were expanded in LB medium with kanamycin. Miniprep was performed on the 2 cultures according to the High Copy number Miniprep protocol (QIAGEN) in order to extract the DNA, and a diagnostic digestion was run to select a clone containing the full CAR (including scFv). On the selected clone and our labs expression vector, Gateway recombination was performed using LR clonase enzymatic mix, producing the expression clone encoding the full humanized CAR, and ampicillin resistance. The expression clone plasmid was transformed into competent NEB5 as prevously described, and plated on LB agar with ampicillin. Colonies were grown, and picked as prevously described, and expanded in LB medium with ampicillin. Finally, miniprep was performed to extract the DNA.

Soluble scFv-IgG's were produced by isolating the humanized scFv, and the backbone of an IgG molecule, using the restriction enzymes NotI-BamHI. The restriction products were run on a 1.5% agarose gel, and the scFv and the IgG backbone were extracted from the gel using the same kit as previously described. Ligation of the scFv and the IgG-backbone was performed as described for production of CARs. Gateway recombination, transformation and miniprep was performed as prevously described.

Protein lysate

One million J76E2 cells transduced with mCAR, hCAR, or non-transduced, were collected and washed in cold DPBS, and pelleted using a microcentrifuge. Lysis buffer was prepared by adding 1 µl protease inhibitor (Thermo Fisher) to 100 µl RIPA (Thermo Fisher), and immediately added to cell pellet. The pellet was resuspended in lysis buffer, and incubated on ice for 20 minutes. The samples were passed though a syringe multiple times before they were centrifuged at

12000/15000 rpm, 4°C, for 20 minutes. The supernatant was collected in eppendorf tubes, and stored long term at -18°C.

Western Blot

Lysates were thawed on ice, before 2x Laemmli sample buffer was added in equal volume. The samples were placed on a 95°C heat block for 5 minutes, before they were loaded into the wells of a mini-PROTEAN TGX 4-20% precast gel (BIO-RAD), with SeeBlue Plus2 protein marker (Invitrogen). The SDS-PAGE was run at 200V/50mA for 30-40 minutes, in 1L of 1x Tris-Glycine SDS running buffer (BIO-RAD). 1x Transfer buffer was prepared by diluting 200 mL 5x Transfer buffer (Invitrogen) in 600 mL nanopure filtered water, and 200mL reagent grade ethanol. For transfer of protein from SDS-PAGE gel to PVDF membrane, the Trans-Blot Turbo Transfer system (BIO-RAD) was used. Transfer stacks were soaked in transfer buffer, and PVDF membrane was equilibrated in 100% methanol, before it was briefly submerged in transfer buffer. The gel was placed on the PVDF membrane, sandwiched in between two transfer stacks, and placed in the transfer cassette. Transfer was run with Turbo Mini TGX program. The membrane was briefly washed in PBST 0.1% (Thermo Fischer), and blocked in PBSTM 5% over night at 4°C on shaker. After blocking, the membrane was repeatedly washed in PBST, before incubation with anti-CD3ζ-IgG (1:1000) (Abcam) in PBSTM for 1.5 hours at room temperature on shaker. Following incubation with the primary antibody, the membrane was repeatedly washed in PBST on shaker, and incubated with anti-IgG-HRP (1:2500) (Invitrogen) at room temperature for 1.5 hours. Following incubation with the secondary antibody, the membrane was repeatedly washed again. For chemoluminescent detection of protein, the Supersignal West Dura substrates (Thermo Fisher) were mixed in equal volumes, and pipetteted onto the membrane. Images were taken with the Amersham Imager.

2.5 Reporter assay

For initial testing of the humanized CARs, a nuclear factor of activated T cells (NFAT)-GFP reporter system was used in J76E2 cells. A NFAT-GFP reporter construct, which was kindly gifted from Peter Steinbergerer (Addgene plasmid # 118031), was transduced into the J76E2 cells devoid of the TCR α- and β-chains to create a reporter system allowing for GFP detection upon activation of the NFAT promoter. Thereafter, the NFAT-GFP-J76E2 cells were transduced

with a vector containing the CAR. This allowed for GFP expression upon CAR induced activation of the NFAT promoter when co-incubated with a target-positive cell line, and quantification of the signal wihtout the interference of TCR GFP-activation signals (illustration 11). For reporter assays by videomicroscopy, the IncuCyte S3 (Sartorious) was used. The adherent target cell line OSA was chemically detached and washed, resuspended to a concentration of $2x10^5$ cells/ mL, and 100 µL was preseeded in each well in a 96 well plate the day before the assay was launched. The following day, J76E2 cells transduced with the original mCAR or hCAR, or non-trasnsduced, were resuspended at $2x10^6$ cells/ mL, from which 100 µL were dispensed in each well under the following conditions: Effector only, Effector and Target, and Effector with PMA/Ionomycin.

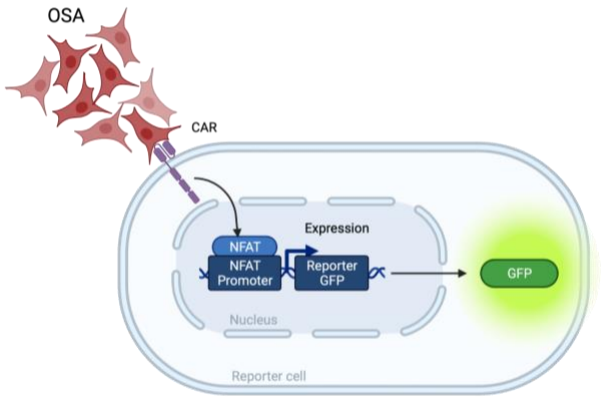

Illustration 11. NFAT reporter system. The illustration shows a simplified pathway, from CAR activation to expression of GFP through the NFAT responsive promoter. Made in Biorender by PA.

PMA and Ionomycin were added to the cells to induce maximum activation, and served as a control for the activation potential of transduced and non-transduced cells. PMA specifically is an activator of Protein kinase C (PKC)[55], while Ionomycin synergistically induces activation of PKC, as well as Ca^{2+}-calmodulin-calcineurin dependent signaling pathways[56].

Plate was left in incubator for 48 hours, with the IncuCyte set to image cells every hour. Experiment was run with duplicates. Effector to target ratio was 10:1.

Table 2. A visual representation of the different conditions in the reporter assays.

E only	Mock (200k)	CAR (200k)
E + T	Mock (200k) + OSA (20k)	CAR (200k) + OSA (20k)
PMA/Iono	Mock (200k) + PMA and Ionomycin	CAR (200k) + PMA and Ionomycin

2.6 Functional assays

Bioluminescence Imaging, killing assay

The adherenrt target cells OSA-GFP-Luc, LM-7-GFP-Luc and HEK-GFP-Luc were chemically detached, washed twice in BLI media and, resuspended at a concentration of $2x10^5$ cells/ mL in BLI media. To each well of a flat bottom optical white 96 well plate (Thermo Fisher), 100 µL was dispensed, and left to adhere in incubator over night. White optical plates were used to avoid spillover of luciferin signal from one well to another. The following day, T cells transduced with either mCAR or hCAR, or non-transduced, were washed twice in BLI media, and resuspended at a concentration of $2x10^6$ cells/ mL, from which 100 µL of T cells were dispensed in each well under the Effector and Target condition. Wells containing only target cells were kept for the minimal cell death (target cells in media), and maximal cell death (target cells in 2% triton) conditions. Luciferin was dispensed (0.0134 M per mL target cells). Bioluminescence was measured and quantified using the Victor x4 Multimode Plate Reader (PerkinElmer) every 2 hours. Experiment was run with triplicates. Effector to target ratio was 10:1.

Table 3: A visual representation of the different conditions in the killing assays.

Mock (200k) + target (20k)	CAR (200k) + target (20k)	Target (20k) in media	Target (20k) in 2% triton

Specific lysis was calculated using the following formula:

$$\frac{Spontaneous\ death\ RLU\ (average) - \ Experimental\ death\ RLU\ (average)}{Spontaneous\ death\ RLU\ (avergae) - \ Maximum\ death\ RLU\ (average)} \cdot 100$$

Degranulation and cytokine production assay

Target cells were washed with flow buffer and adjusted to $2x10^6$ cells/ mL in plain X-vivo 15, from which 100 µl were dispensed in each well of a 96 well plate, the day before assay launch. Effector cells transduced with mCAR, hCAR or non-transduced, were washed in flow buffer adjusted to $2x10^6$ cells/ mL in plain X-vivo 15, from which 50 µl were dispensed on top of pre-seeded target cells under the following conditions: Effector only, Effector and Target, and Effector with PMA/Ionomycin. A master mix of the following antibodies was prepared: anti-CD107a (0.0063 µg/sample)(Clone H4A3, BD Biosciences), GolgiPlug (BD Biosciences) (1/1000), and GolgiStop (BD Biosciences) (1/1000).From this master mix 10.4 µl were added to each well, and each well was subsequently topped off with 36.5 µl plain X-vivo 15, resulting in a total volume of 200 µl/well. PMA (1/10 000) and Ionomycin (1/1000) was dispensed in each well under control condition.

Table 4. A visual representation of the different conditions in the degranulation and cytokine release assays.

E only	Mock (100k)	CAR (100k)
E + T	Mock (100k) + OSA (200k)	CAR (100k) + OSA (200k)
PMA/Iono	Mock (100k) + PMA and Ionomycin	CAR (100k) + PMA and Ionomycin

Plate was incubated for 7 hours, and placed in fridge overnight. Effector to target ratio, 1:2. Experiment was run with duplicates. The following day, the cells were permeabilized and fixed (PerFix-nc kit from Beckman Coulter) and intracellular staining was performed. Each sample was resuspended in 50 µl FBS, and 2.5 µl of fixative agent R1 were added to each tube before vortexing immediately. Samples were incubated at room temperature for 15 minutes, before they were vortexed again, topped off with 150 µl of permeabilizing agent R2, and vortexed immediately. A master mix of the following antibodies was prepared: anti-CD4 (0.0175µg/sample) (BD Biosciences), anti-CD8 (0.03 µg/sample) (BD Biosciences) and anti-TNF-α (0.003 µg/sample) (BD Biosciences). Fifteen µL of the antibody master mix was added to each sample, and then samples were vortexed and incubated at room temperature for 30 minutes. Samples were then washed in reagent R3 diluted in nanopure H_2O, centrifuged at 400xg for 5 minutes, and resuspended in a final volume of 300 µl. Staining efficiency was detected on Flow cytometer.

Exhaustion assay

T cells transduced with mCAR, hCAR or non-transduced, were stained for CAR expression by anti-CD34 staining, and cell count and viability was recorded. CAR T cells and non-transduced T cells were then used for killing assays, as previously described. Feeder cells (LM7) were irradiated, centrifuged at 500xg for 5 minutes, and resuspended in T cell media before being added to cell suspension in ratio 1:2, Effector cells: Feeder cells. Cell suspension was incubated for 3-4 days, before they were counted and re-adjusted to a concentration of $1x10^6$ T cells/ mL. Seven days after the first feeding of irradiated LM7 cells, T cells were again stained for CAR

expression, cell count and viability was recorded, BLI was again performed, and T cells were re-stimulated with irradiated feeder cells. This cycle was repeated for 4 weeks.

3. Results

Preliminary testing of the OS- and OF- series in J76E2 cells

After J76E2 cells were transduced with murine OSCAR-1 and -3, and humanized constructs from the OS- and OF-series, they were expanded for 10 days (figure 1). Expansion was recorded and analyzed in order to assess the potential toxicity of each humanized construct, in comparison to the murine OSCAR-1 and OSCAR-3. The original OSCAR-1 and -3 showed no unexpected toxicity in PBMCs, but with introduction of humanized consesus sequenes, the expansion of cells transduced with the humanized constructs required assesment. Cellular expansion was expected to be similar between mCAR and hCAR transduced cells if the toxicity profile of the CAR had not been altered by the humanization of the scFv. The humanized constructs OS3-4, OF1-2 and OF3-1 affected expansion of J76E2 cells negatively. In conclusion, the cells transduced with constructs OS3-4, OF1-2 and OF3-1 expanded considerably slower than their murine counterparts, which may indicate an increase in toxicity introduced with the humanized sequence.

Figure 1.

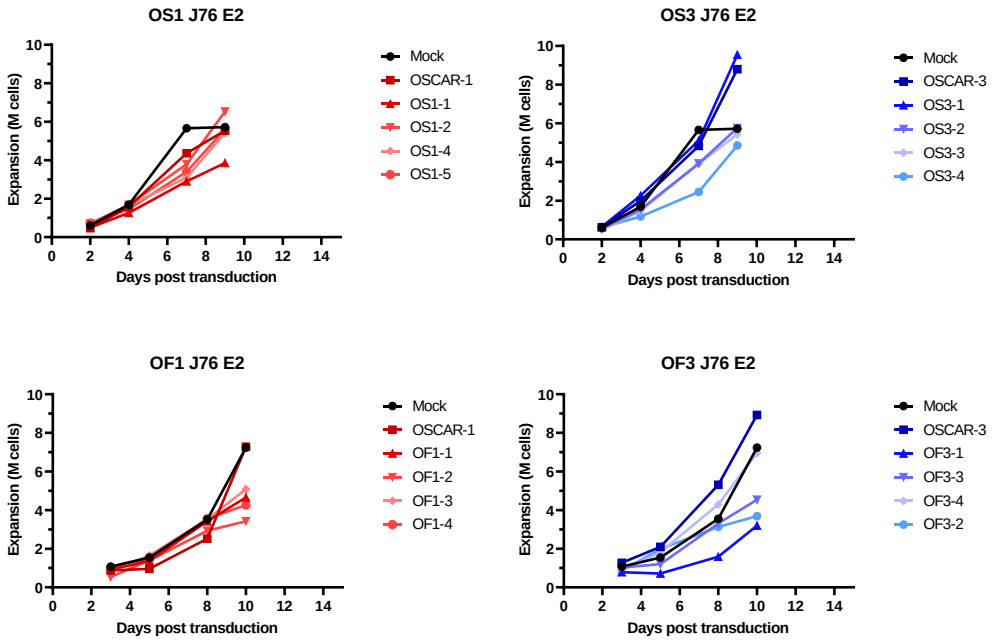

Figure 1: Expansion of transduced or non-transduced J76E2 cells. Expansion curves of J76E2 cells transduced with OSCAR1, OSCAR3 or humanized OSCAR1 and -3 from the OS- and OF-series.n=1.

The J76E2 cells transduced with OSCAR-1, OSCAR-3 and the 2 humanized series were stained with goat anti-mFab to investigate if humanization of the scFv had resulted in reduced recognition compared to the original mCARs (figure 2a, 2b). The recognition of mFab was expected to be reduced in the humanized constructs, because parts of the murine scFv amino acid sequence were replaced by human consesus sequences. Murine OSCAR-1 were up to 28% positive for mFab, the humanized OS-1 constructs were all more positive for mFab than OSCAR-1 – ranging from up to 32% to 94% - while the humanized OF-1 constructs maintained a similar mFab recognition profile to OSCAR-1. From the humanized OS-1 constructs, OS1-2 and OS1-4 showed the highest mFab recognition with up to 94% and 75% positive cells respectively. Murine OSCAR-3 was up to 99% positive for mFab, the humanized OS-3 constructs ranged from 20-100% positive for mFab, and the humanized OF-3 constructs were all drastically less positive for mFab, staining up to only 17% positive. The increased recognition of mFab observed in the humanized OS-1 constructs was not expected. The preserved mFab recogition profile observed in the OF-1 constructs, and the decreased mFab recognition profiles of the OS-3 and OF-3 constructs were expected as a result of the humanization of the scFvs. In conclusion, humanization of the original murine scFvs did not consistently reduce the recognition of mFab.

Figure 2a.

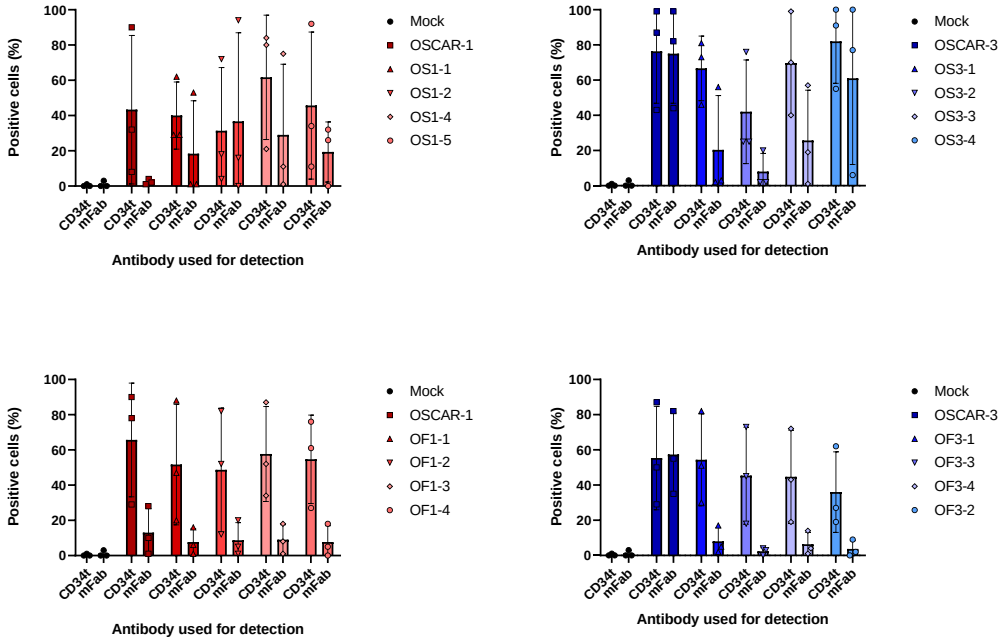

Figure 2a: Transduction efficiency. Average transduction efficiency of humanized and murine OSCAR-1 and OSCAR-3 in J76E2 cells measured by expression of truncated CD34 (CD34t) and mFab. n=3.

Figure 2b.

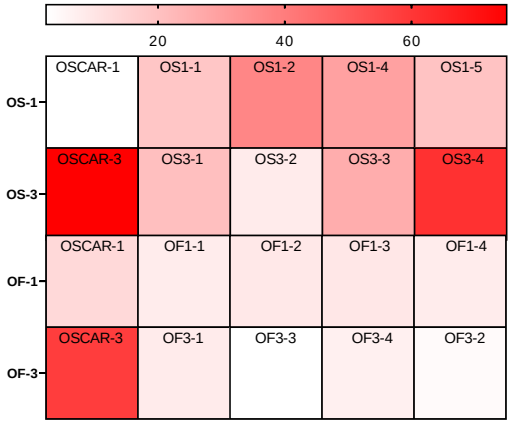

Figure 2b: mFab recognition heat map. Heat map of mFab recognition in J76E2 cells transduced with OSCAR-1 and -3, and the OS- and OF-series. Plotted is the average recognition of mFab from 3 transductions. n=3

To investigate if the humanized scFvs had preserved the ability to recognize and bind the target molecule, and initiate the intracellular signaling pathway resulting in induction of the NFAT responsive promoter, the original and humanized CARs were co-incubated with a target positive cell line for 40 hours (figure 3). The murine OSCAR-1 and OSCAR-3 had not previously been tested in this NFAT reporter system, but were expected to show increased NFAT-GFP signaling over the first 24 hours, demonstrating reactivity against the target molecule expressed on the cell line OSA. If the reactivity had been preserved in the humanized constructs, the NFAT-GFP signal was expected to be comparable between the mCARs and the hCARs, if not increased due to stabilization of the hCARs. The J76E2 cells transduced with OSCAR-1 showed minimal activation with an increase in Green Mean Intensity (GMI) of approximately 1 unit when co-incubated with OSA in IncuCyte, still the activation was higher than mock. OSCAR-3 showed clear activation with an increase in GMI of 4-5 units when co-incubated with OSA. The humanized OS-1 constructs showed an increase in GMI comparable to OSCAR-1, and the humanized OS-3 constructs showed clear activation, with an increase in GMI somewhat lower than OSCAR-3. The humanized OF-1 and OF-3 constructs showed no GFP-activation when co-incubated with OSA. The difference in GFP activation signal intensity observed between OSCAR-1 and -3 was unexpected, but both CARs had prevously demonstrated reactivity against OSA in other experiments.

Figure 3.

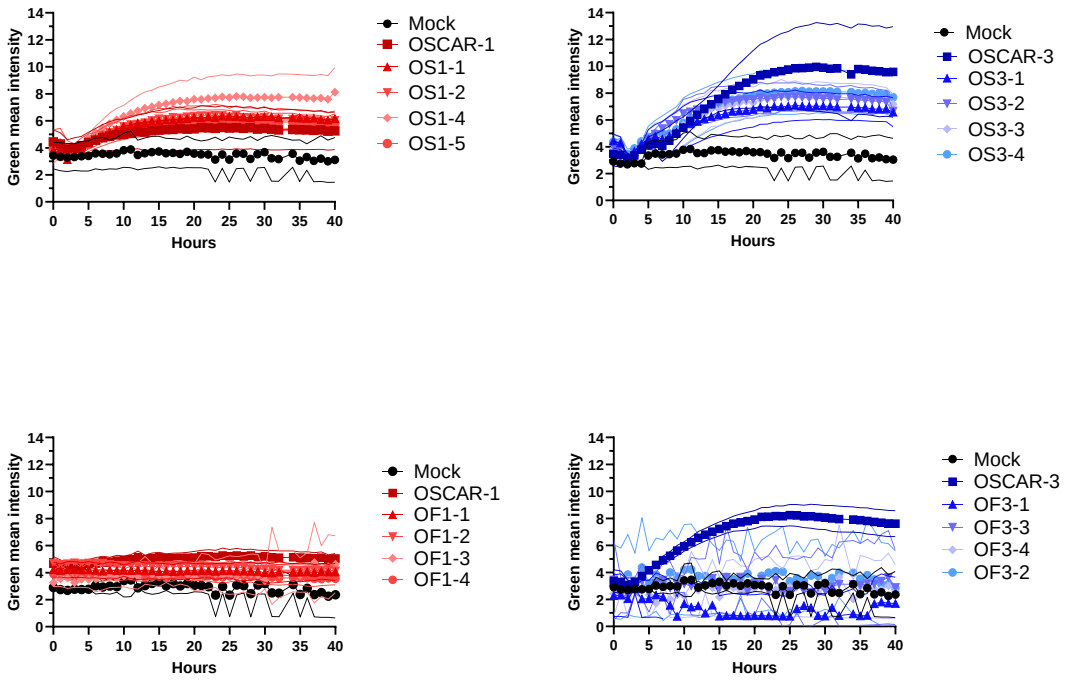

Figure 3: NFAT reporter assays. NFAT reporter assay in IncuCyte with J76E2 cells transduced with murine or humanized OSCAR-1 and OSCAR-3, or non-transduced, CAR activation measured and quantified by Green Mean Intensity. OS series: n=4-7. OF series: n= 4-5.

Images from co-incubation with OSA after 24 hours show NFAT-GFP activation of single cells transduced with OSCAR-1, OSCAR-3, humanized constructs OS1-1 and OS3-2, but no single cell NFAT-GFP activation in humanized constructs OF1-1 and OF3-3 after 24 hours (figure 4). Images show that considerably more OSCAR-3-and OS3-2-transduced cells are NFAT-GFP activated, compared to OSCAR-1- and OS1-1- transduced cells. In conclusion, the OS-1 and OS-3 series demonstrated comparable NFAT-GFP activation signal to OSCAR-1 and OSCAR-3, respectively, and the OF-1 and OF-3 series demonstrated no NFAT-GFP activation in this experiment.

Figure 4.

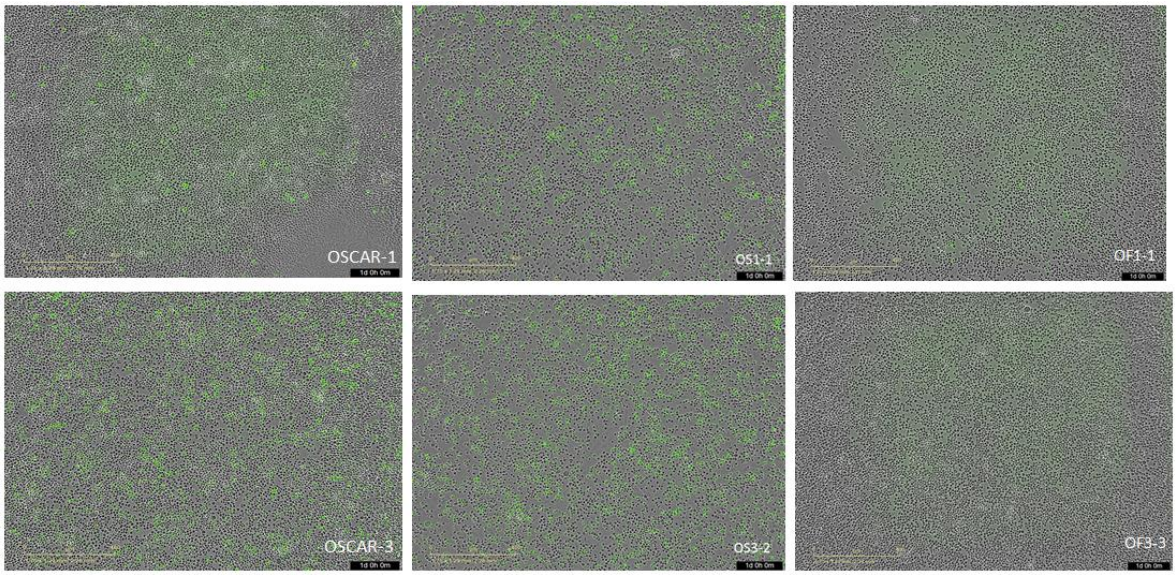

Figure 4: Live microscopy images. IncuCyte images of OSCAR-1, OS1-1, OF1-1, OSCAR-3, OS3-2 and OF3-3 after 24 hours co-incubation with OSA.

Based on the NFAT-GFP activation signal intensities recorded in the IncuCyte, the humanized OS-3 constructs appered to have preserved a comparable antigen binding affinity to their original murine counterparts. To asses wether the effective concetration of the hCARs had been altered from OSCAR-3, non-linear regression (curve fit) analysis was performed and EC50 was calculated with graphpad (figure 5). There was no statistically significant difference in EC50 between OSCAR-3 and the humanized OS-3 constructs.

Figure 5.

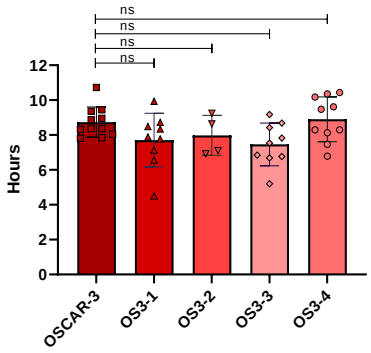

Figure 5: EC50 calculation. EC50 calculated on OSCAR-3 and humanized OSCAR-3 from OS series by non-linear regression (curve fit), one-way ANOVA analysis and multiple comparisons (OSCAR-3 VS. OS3-1/ OS3-2 / OS3-3/ OS3-4). n=4-11.

Comparison of NFAT GFP activation signal between OSCAR-1 and OSCAR-3

The stark difference in NFAT-GFP signal intensity between OSCAR-1 and OSCAR-3 during co-incubation with OSA was unexpected, and prompted further testing with a lower E:T ratio, supplemented with NFAT-GFP signal singel cell analysis with flow cytometry. If the cause of the low signaling intensity observed in OSCAR-1 was insufficient antigen density, increasing the target ratio was expected to elevate the NFAT-GFP signal intensity. Singel cell analysis of NFAT-GFP activation with Flow cytometry was used as an additional mean of detection with a higher sensitivity compared to IncuCyte imaging and calculation of GMI (figure 7a, 7b). J76E2 cells transduced with OSCAR-1 and -3, or non-transduced, were co-incubated with OSA at Effector: Target ratios 10:1 and 1:2. OSCAR-3 showed clear activation at both ratios with an increase in GMI of approximately 3 units, and OSCAR-1 showed minimal activation at 1:2 ratio with an increase in GMI of approximately 1 unit, and no increase in GMI at ratio 10:1.

Figure 7a.

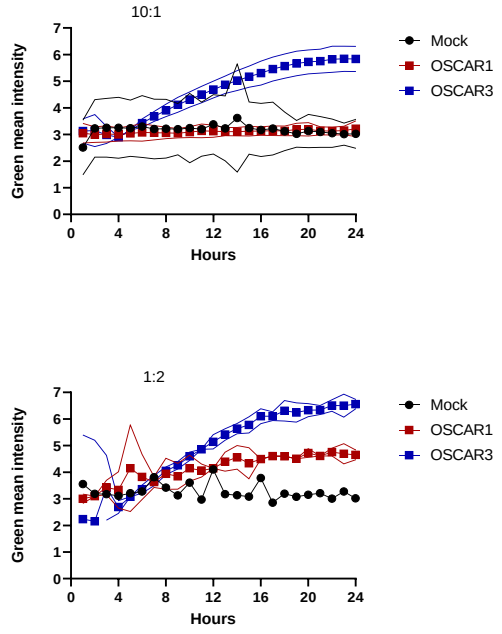

Figure 7a: NFAT reporter assay. NFAT reporter assays of OSCAR-1 and -3, co-incubated with OSA for 24h. Effector to target ratio 10:1, n=8. Effector to target ratio 1:2, n=2.

CAR expression was measured before co-incubation with anti-CD34t staining, and NFAT-GFP activation was measured on flow cytometry before and after 24 hours co-incubation with OSA.

OSCAR-3 showed clear elevation in NFAT-GFP after 24 hours co-incubation with OSA, with increase from 0% CD34t+GFP+ cells at 0 hours, to 40-60% CD34t+GFP+ cells at 24 hours. OSCAR-1 showed no elevation in CD34t+GFP+ cells after 24 hours co-incubation with OSA. In conclusion, these results indicate that OSCAR-1 NFAT-GFP activation signal can not be detected on Flow cytometry or on the IncuCyte.

Figure 7b.

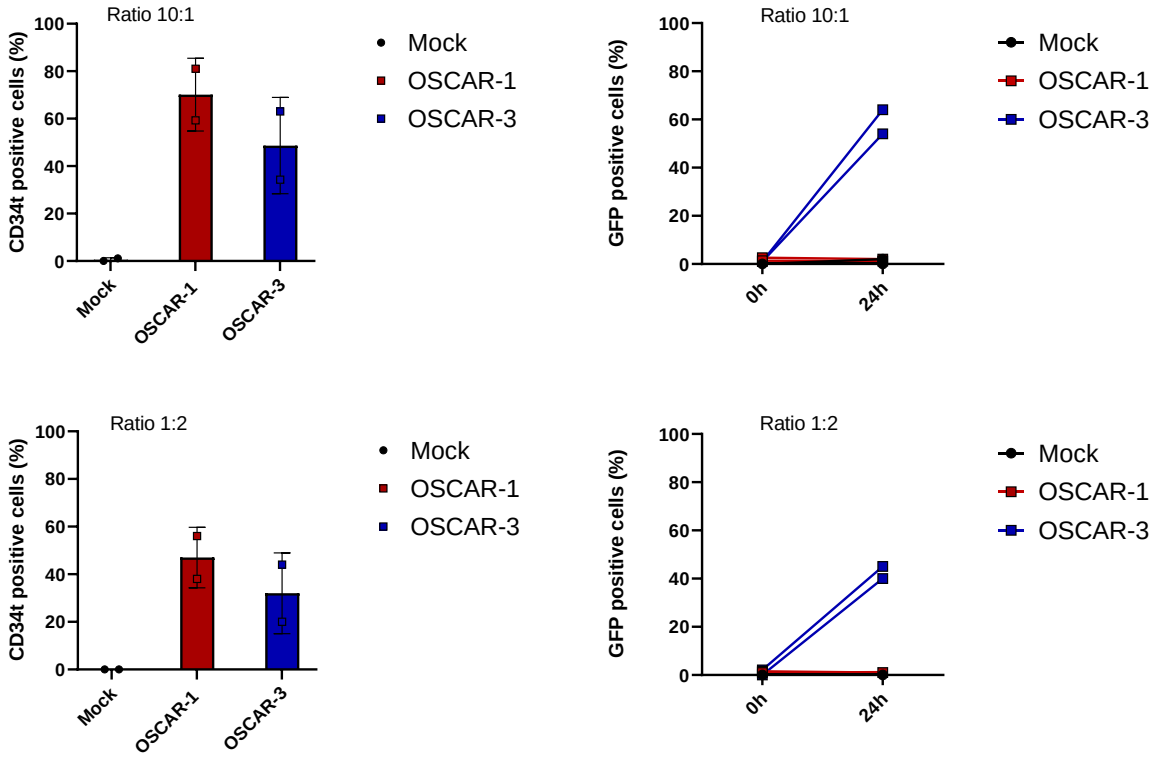

Figure 7b: CAR expression and NFAT-GFP activation signal. CAR expression, detected by truncated CD34, and CAR activation, measured by GFP signal from CD34t+ cells, measured with flow cytometry before and after 24 hours of co-incubation with OSA. Effector to target ratio 10:1, n=2. Effector to target ratio 1:2, n=2.

Investigating the nature of the OF-series lost reactivity against OSA

The OF-series´ lack of NFAT-GFP activation signal during co-oincubation with OSA warranted investigation into the cause of the lack of reactivity. The lack of reactivity against the target molecule could be due to destabilization or degradation of the CAR protein, and western blot was performed to investigate if the humanized OF constructs were translated into protein, and expressed at similar levels to the original OSCARs (figure 6a, 6b, 6c). If humanization of the scFvs had led to destablization or degradation of the protein, the intensity of the bands corresponding to the hCARs were expected to be lower than the bands corresponding to the mCARs, or not detectable at all. Western blot of J76E2 cells transduced with OSCAR-1 and -3 and humanized OF series, or non-transduced, show that the humanized OSCARs were transcribed and translated into protein in these cells. The mCAR and hCAR protein expression levels were comparable to the endogenous CD3ζ level. Only one construct, the OF1-1, was detected at a higher intensity than the original murine counterpart OSCAR-1. These results show that the original and humanized CARs were translated into protein in J76E2 cells, and indicate that the lact of reactivity obeserved from the OF-series in the NFAT reporter assay was likely not due to destabilization or degradation of the humanized proteins.

Figure 6a.

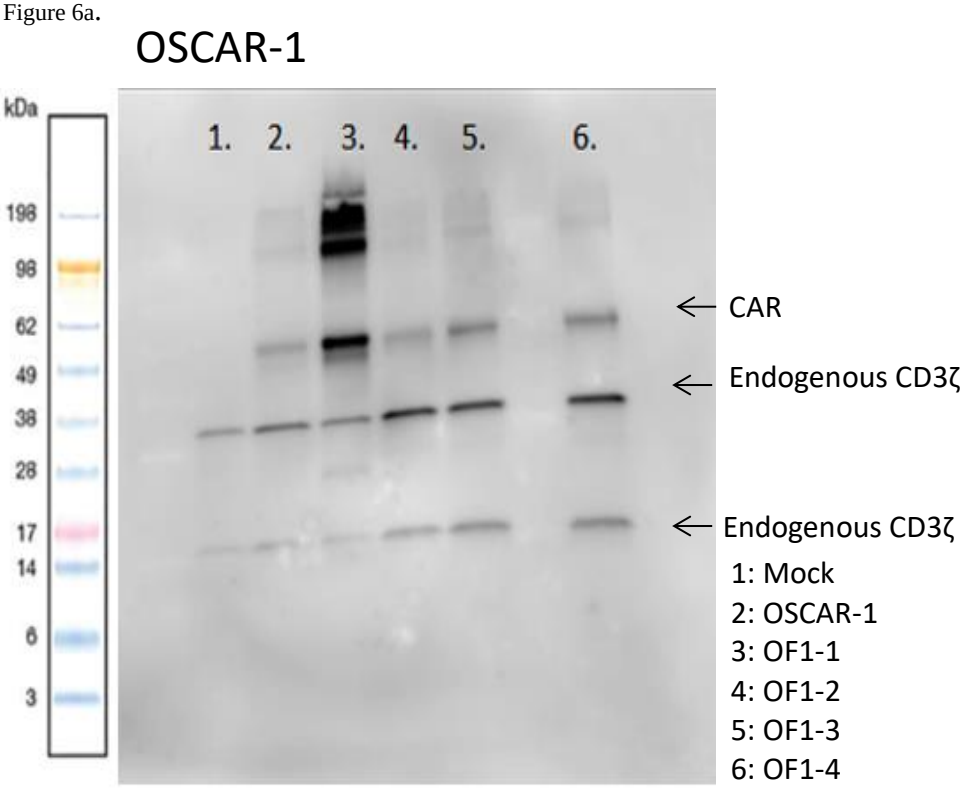

Figure 6b.

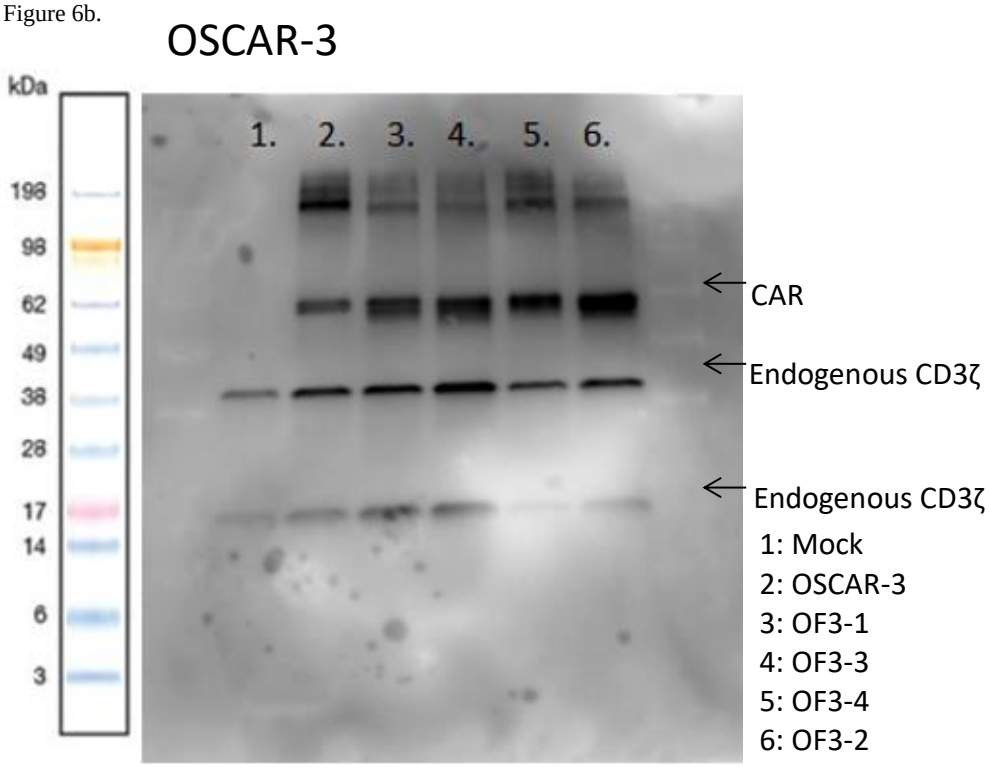

Figure 6c.

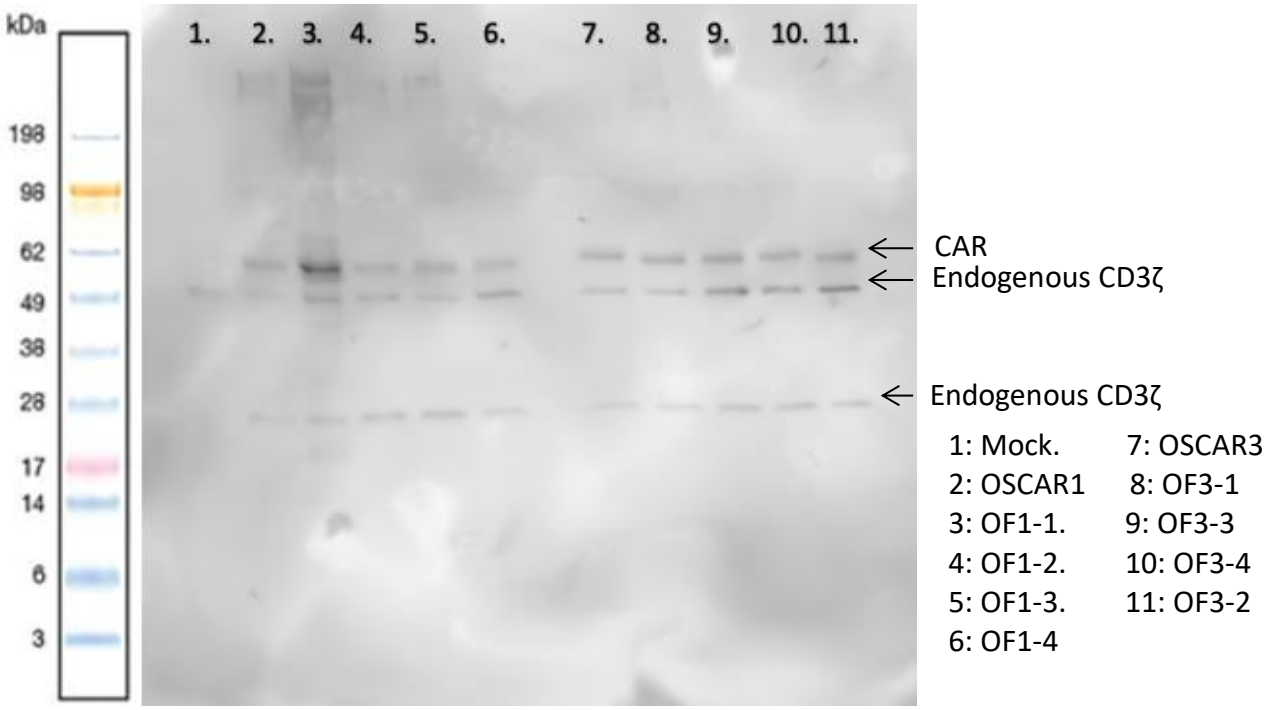

Figure 6a and 6b: OF CARs detected in Western Blot. Western blot of J76 E2 cells transduced with OSCAR-1 and -3 with corresponding humanized constructs from the OF-series.. Figure 6c: Western blot of J76 E2 cells transduced with OSCAR-1 and -3, and all humanized constructs from the OF-series. Fig. 6a-c: Non-reducing conditions, stained with primary antibody anti-CD3ζ-IgG, followed by secondary antibody anti-IgG-HRP

After detection of the OF-series hCAR proteins in J76E2 cells with western blot, investigation into the target recognition and binding efficacy of the scFvs was performed (figure 8a, 8b). Alterations in the amino acid sequence of the scFv may affect the folding of the antigen-binding domain of the CAR protein, or result in mismatch between amino acids in the epitope-paratope interface, depending on the position of the mutation in the scFv sequence. If humanization of the OF-series scFvs had disrupted the antigen recognition by either cause, incubation of target positive cells with scFv-IgGs and assesment of binding efficacy with Flow Cytometry was expected to result in a lowered percentage of positive cells compared to the murine scFv-IgG. If the humanization had not disrupted the antigen recognition, but rather the signal transduction through the scFv, the flow cytometry analysis was expected to result in a high percentage of positive cells. OSCAR-3, the OS3-3, OF3-4 and OF3-2 humanized scFvs were cloned into soluble IgG's, and produced in HEK-P cells. Western blot of the supernatant from the scFv-IgG production showed that they had been produced successfully. The bands were quantified using GelQuant.net software provided by biochemlabsolutions.com. Quantification of the protein bands showed that the level of OSCAR-3-IgG, OS3-3-IgG and OF3-2-IgG were comparable. The OF3-4-IgG was produced at a drastically lower level.

Figure 8a.

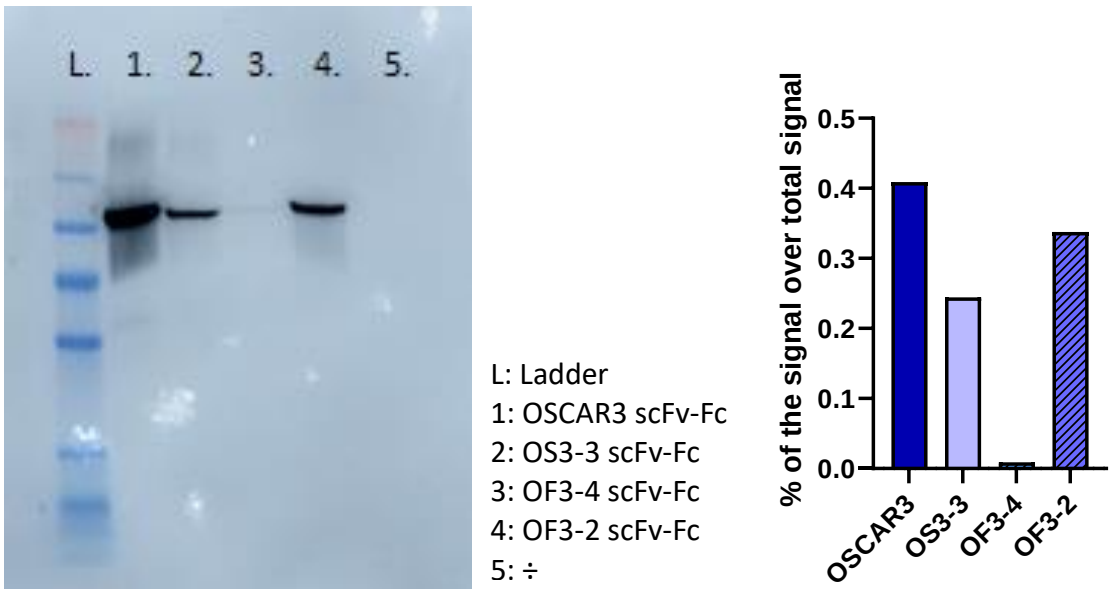

Figure 8a: ScFv-IgGs detected in Western blot. Western blot of scFv-IgG supernatant stained with anti-IgG-HRP, and quantification of the band intensities.n=1.

The OSCAR-3-, OS3-3-, OF3-4- and OF3-2-IgG's were incubated with chemically detached OSA, followed by incubation with a secondary IgG-APC antibody for detection with flow cytometry. The staining showed that OSCAR-3-IgG and OS3-3-IgG recognized and bound OSA cells, but the OF3-2-IgG and OF3-4-IgG were not able to recognize or bind these cells.

Figure 8b.

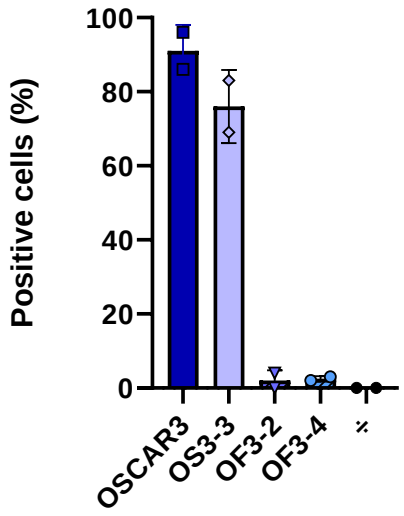

Figures 8b: ScFv-IgG staining efficiency. Primary scFv-IgG staining, and secondary IgG-APC staining on OSA cells, staining quantified by flow Cytometry. n=2.

In conclusion, these results indicate that the humanization of the OF-series scFvs had disrupted the antigen affinity, and the OF-series was excluded from further testing in PBMCs.

In vitro experiments in PBMCs transduced with the OS-series

Following preliminary testing in J76E2 cells, the OS-series were transduced into PBMCs for functional experiments. The expansion of the PBMC's from 5 healthy donors transduced with OSCAR-1 and -3, and the humanized OS-series, or non-transduced, was recorded for 11-12 days to assess the constructs´ toxicity in primary T cells (figure 9a, 9b). When expansion curves from the 5 donors where pooled by constructs, unpaired t test showed a statistically significant difference in expansion only between mock and OS1-4, and mock and OS1-5. There was no statistically significant difference in expansion between the original OSCAR-1 and mock, nor the original OSCAR-1 and the humanized OS1 constructs.

Figure 9a.

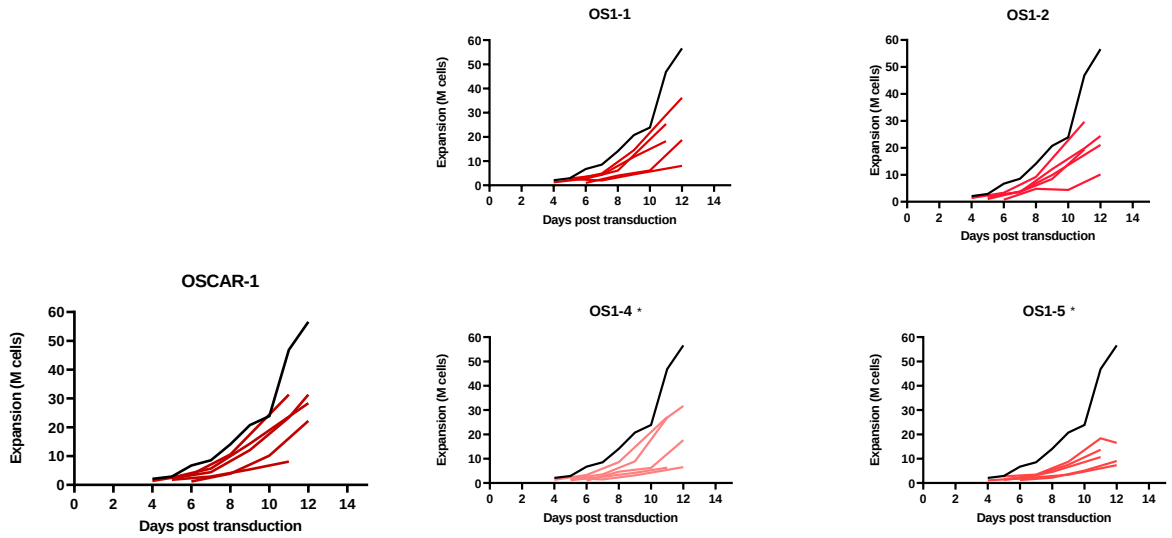

Figure 9a: Expansion OS-1 in PBMCs. Expansion curves of T cells from 5 different donors transduced with OSCAR-1 or humanized OSCAR-1 OS-series. Unpaired t test of expansion average of mock across 5 donors (black curve) VS. expansion average of 5 donors pooled show no statistically significant difference between OSCAR-1/ OS1-1/ OS1-2 and mock, but statistically significant difference between OS1-4 and mock, and OS1-5 and mock (marked with *). Unpaired t test of average of OSCAR-1 VS. OS1-1/ OS1-2/ OS1-4/ OS1-5 showed no statistically significant difference.

Unpaired t test showed a statistically significant difference in expansion only between mock and OS3-3, and not between OSCAR-3 and mock, nor OSCAR-3 and the humanized OS3 constructs. In conclusion, these results may indicate that constructs OS1-4, OS1-5 and OS3-3 have a higher tocixity in PBMCs compared to their original counterpart.

Figure 9b.

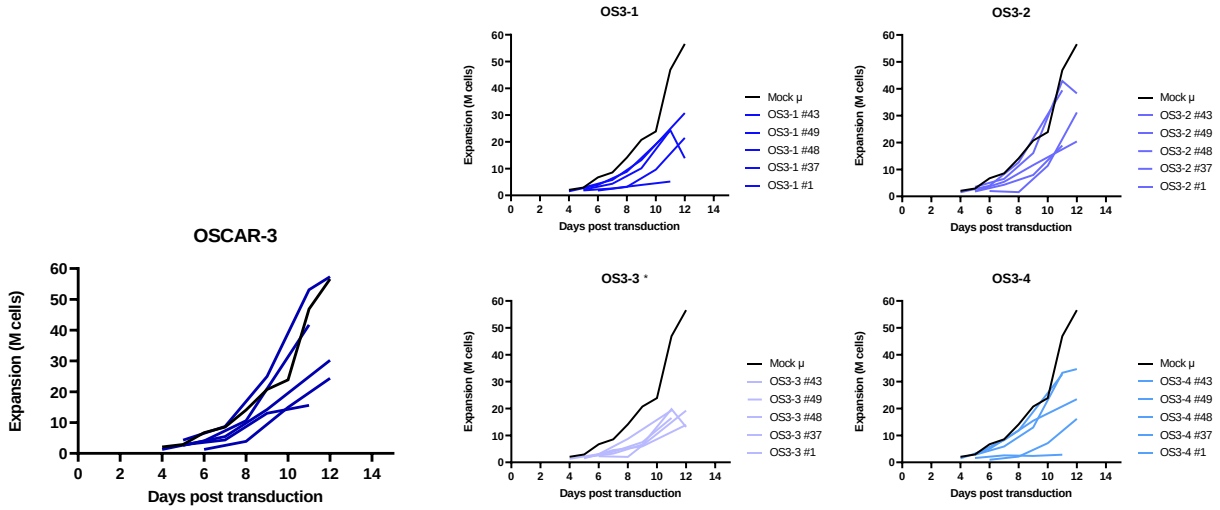

Figure 9b: Expansion of OS-3 in PBMCs. Expansion curves of T cells from 5 different donors transduced with OSCAR-3 or humanized OSCAR-3 OS-series. Unpaired t test of expansion average of mock across 5 donors (black curve) VS. expansion average of 5 donors pooled show no statistically significant difference between OSCAR-3/ OS3-1/ OS3-2/ OS3-4 and mock, but statistically significant difference between OS3-3 and mock (marked with *). Unpaired t test of average of OSCAR-3 VS. OS3-1/ OS3-2/ OS3-3/ OS3-4 showed no statistically significant difference.

After 11-12 days of expansion, the T cells' CAR expression was measured on flow cytometry by CD34t and mFab expression (figure 10a, 10b), and cut off to be included in the functional assays were set at 60% CD34t. As prevously described, mFab recognition was measured to assess humanization. OSCAR-1 T cells were no more than 18% positive for mFab, while OSCAR-3 were up 63% positive for mFab. The humanized OS1 constructs showed low mFab recognition similar to OSCAR-1, except for OS1-4 which showed increased mFab recognition of up to 34%. The humanized OS3 constructs all showed decreased recognition of mFab compared to OSCAR-3, with recognition ranging from 0-37% positive cells. In conclusion, these results indicate that the humanization of the scFv may have reduced the immunogenic potential of all the hCARs from the OS3-series, and mostly preserved the immungeic potential of the OS1-series despite humanization. OS1-4 unexpectedly showed increased recognition of mFab compared to murine

OSCAR-1, possibly indicating enhanced immunogenic potential despite increasing similarity to human heavy and light chain consesus sequences.

Figure 10a.

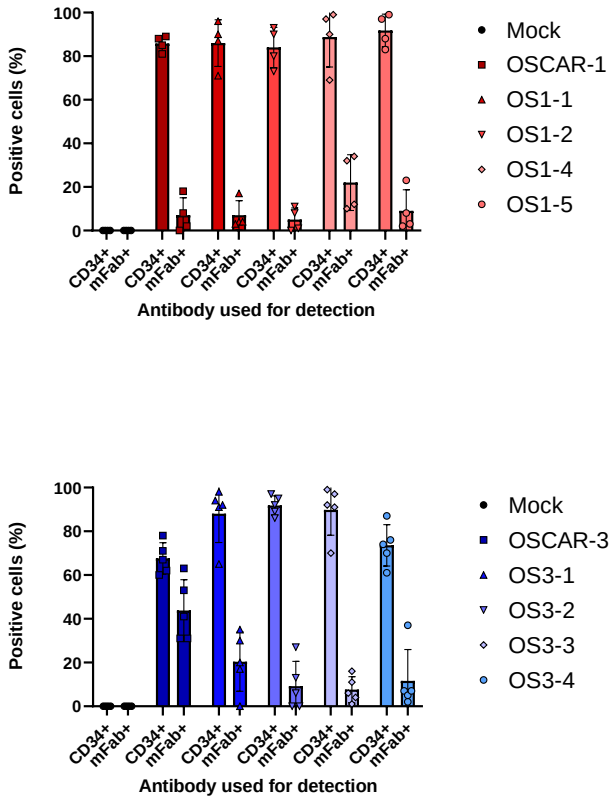

Figure 10a: Transduction efficiency in PBMCs. Expression of OSCAR-1 and -3, and humanized OSCAR-1 and -3 from OS-series, in T cells from 5 healthy donors, detected by CD34t and mFab with flow cytometry.

Figure 10b.

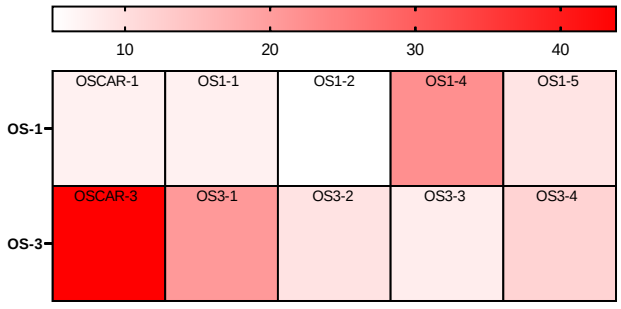

Figure 10b: Heat map of mFab recognition in PBMCs. Heat map of mFab recognition in PBMCs from 5 healthy donors transduced with OSCAR-1 and -3 and the OS-series. Plotted is the average mFab recognition of the 5 healthy donors.

Comparing the cytotoxic efficacy between mOSCARs and hOSCARs

To compare the cytotoxic efficacy of the hCARs compared to the mCARs against target positive cell lines OSA and LM-7, bioluminescent imaging assays were performed (figure 11a, 11b, 11c, 11d). The target negative cell line HEK was included to assess the specificity of the CARs. The humanization of the scFvs was expected to stabilize the CAR protein, thereby potentially increasing the cytotoxic efficacy compared to the mCARs. The following killing assays were analyzed with unpaired, parametric one way-ANOVA. After 8 hours, no statistically significant difference between mock, murine and humanized OSCAR-1 vs. OSA, LM7 and HEK at 2.5:1 ratio was observed. At 10:1 ratio, there was a statistically significant difference between mock and OSCAR-1 vs. OSA and LM7, but no statistically significant difference between OSCAR-1 and humanized OS-1 constructs. At 10:1 ratio, there was still no statistically significant difference between mock, OSCAR-1 and the humanized OS-1 constructs vs. HEK.

Figure 11a.

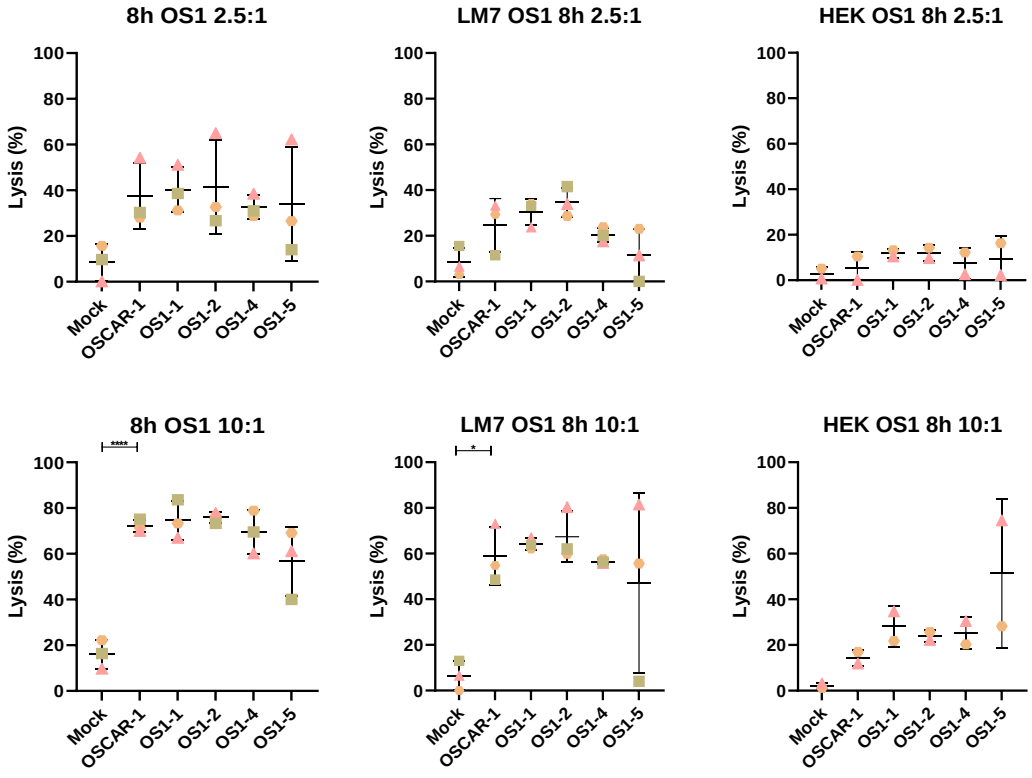

Table 5. The calculated average killing of OSA at ratio 10:1, after 8 hours, by construct.

	Mock	OSCAR-1	OS1-1	OS1-2	OS1-4	OS1-5
Average killing OSA (%) 10:1, 8h	16.0	72.1	75.6	75.8	69.4	56.6

After 8 hours, no statistically significant difference between mock, OSCAR-3 and the humanized OS-3 constructs vs. OSA, LM7 and HEK at 2.5:1 ratio was observed. At ratio 10:1, there was a statistically significant difference in killing between mock and OSCAR-3 vs. OSA and LM7, but no difference between OSCAR-3 and humanized OS-3 constructs. At 10:1 ratio, there was still no statistically significant difference between mock, OSCAR-3 and humanized OS-3 constructs vs. HEK.

Figure 11b.

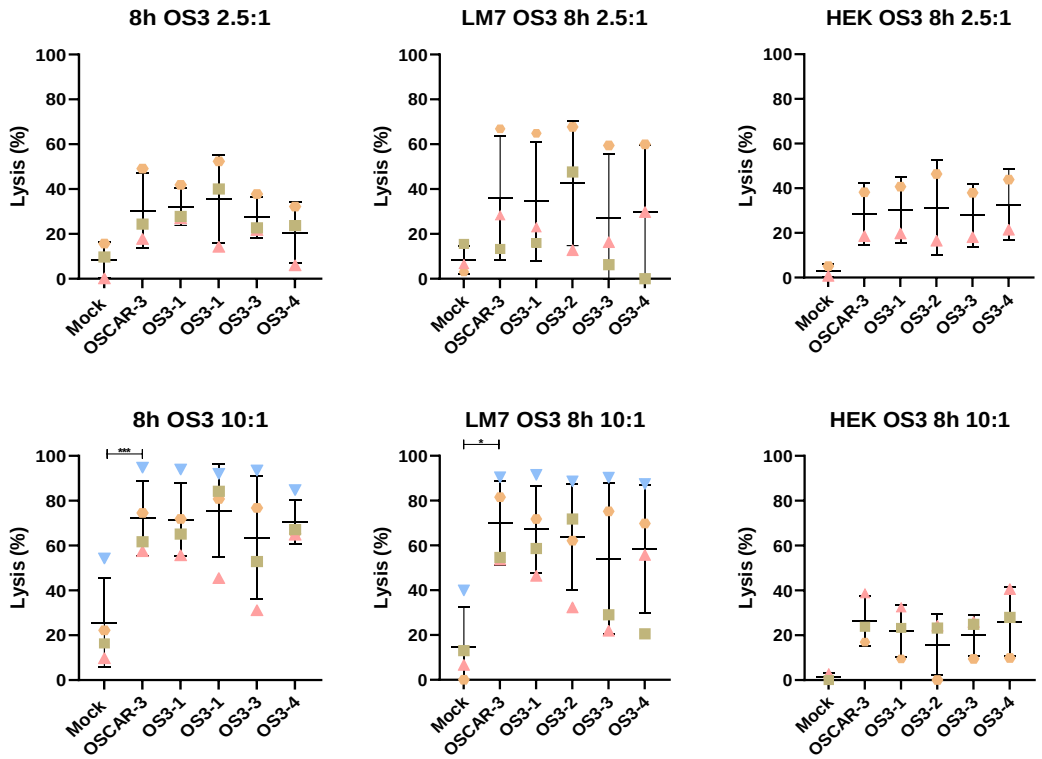

Table 6. The calculated average killing of OSA at ratio 10:1, after 8 hours, by construct.

	Mock	OSCAR-3	OS3-1	OS3-2	OS3-3	OS3-4
Average killing OSA (%) 10:1, 8h	16.0	72.1	71.6	75.6	63.5	70.5

After 24 hours, there was a statistically significant difference in killing between mock and OSCAR-1 against OSA and LM7 at 2.5:1 ratio, but no difference between OSCAR-1 and humanized OS-1 constructs. There was no statistically significant difference between mock, OSCAR-1 and humanized OS-1 constructs vs. HEK at 2.5:1 ratio. At 10:1 ratio, there was a statistically significant difference in killing between mock and OSCAR-1 vs. OSA, LM7 and HEK, but no difference between OSCAR-1 and the humanized OS-1 constructs.

Figure 11c.

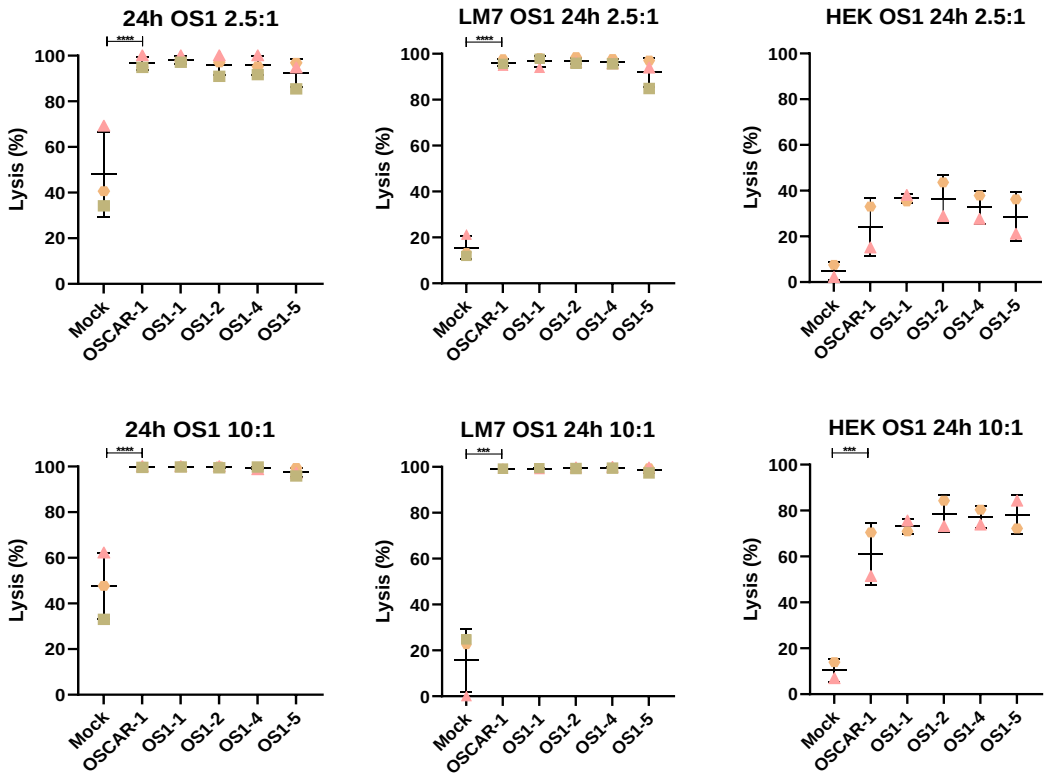

Table 7. The calculated average killing of OSA at ratio 2.5:1, after 24 hours, by construct.

	Mock	OSCAR-1	OS1-1	OS1-2	OS1-4	OS1-5
Average killing OSA (%) 2.5:1, 24h	48	96.6	98.2	96.0	95.6	92.3

After 24 hours, a statistically significant difference in killing between mock and OSCAR-3 vs. OSA and LM7 at ratio 2.5:1 was observed, but not between OSCAR-3 and the humanized OS-3 constructs. No difference was observed between mock, OSCAR-3 and humanized OS-3 constructs vs. HEK at this ratio. At 10:1 ratio, a statistically significant difference between mock and OSCAR-3 vs. OSA, LM7 and HEK was observed, but not between OSCAR-3 and the humanized OS-3 constructs.

Figure 11d.

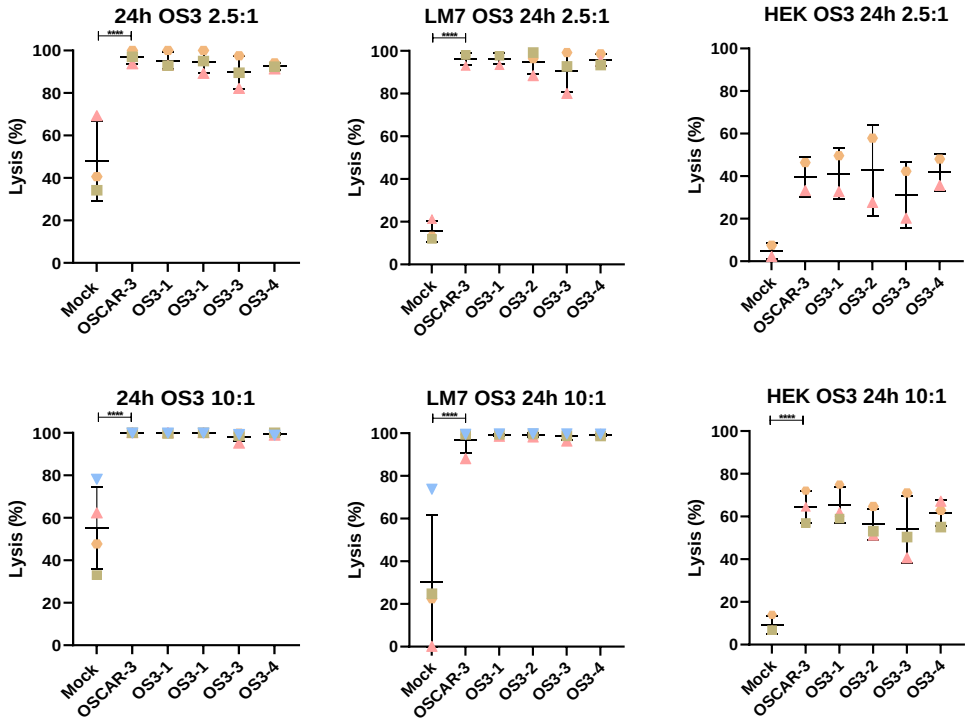

Table 8. The calculated average killing of OSA at ratio 2.5:1, after 24 hours, by construct.

	Mock	OSCAR-3	OS3-1	OS3-2	OS3-3	OS3-4
Average killing OSA (%) 2.5:1, 24h	48	96.9	95.2	94.7	89.7	92.5

Figure 11a, 11b, 11c and 11d: Killing assays. Killing assay with OSCAR-1 and -3, and humanized OSCAR-1 and -3 from OS-series VS. OSA, LM7 and HEK, ratios 2.5:1 and 10:1, after 8h and 24 hours co-incubation. One-way ANOVA, unpaired, unparametric, with multiple comparisons (OSCAR-1 VS. mock /OS1-1/ OS1-2/ OS1-4/ OS1-5) (OSCAR-3 VS. mock/ OS3-1/ OS3-2/ OS3-3/ OS3-4) showed statistically significant difference between mock and OSCAR-1/ OSCAR-3, but not between murine and humanized OSCARs. Statistically significant differences denoted with asterix: *=P 0.0354/0.0200, ***=P 0.0007/0.0005/0.0002, ****=P<0.0001.

Based on the calculated average killing of OSA, at the lowest ratio where the difference between mock and OSCAR-1 and -3 is statistically significant, the humanized construct OS1-4 is most similar to OSCAR-1, and OS3-1 is most similar to OSCAR-3 *in vitro*. Noteably, there was no statistically significant difference between mCARs and hCARs observed in these experiments, indicating that the humanization of the scFvs had not increased the CARs cytotoxic efficacy to an extent where it was observeable in this 24-hour killing assay.

Comparing degranulation and cytokine release between hOSCARs and mOSCARs

Figure 12a shows the gating strategy for the following cytokine release and degranulation assay.

Figure 12a

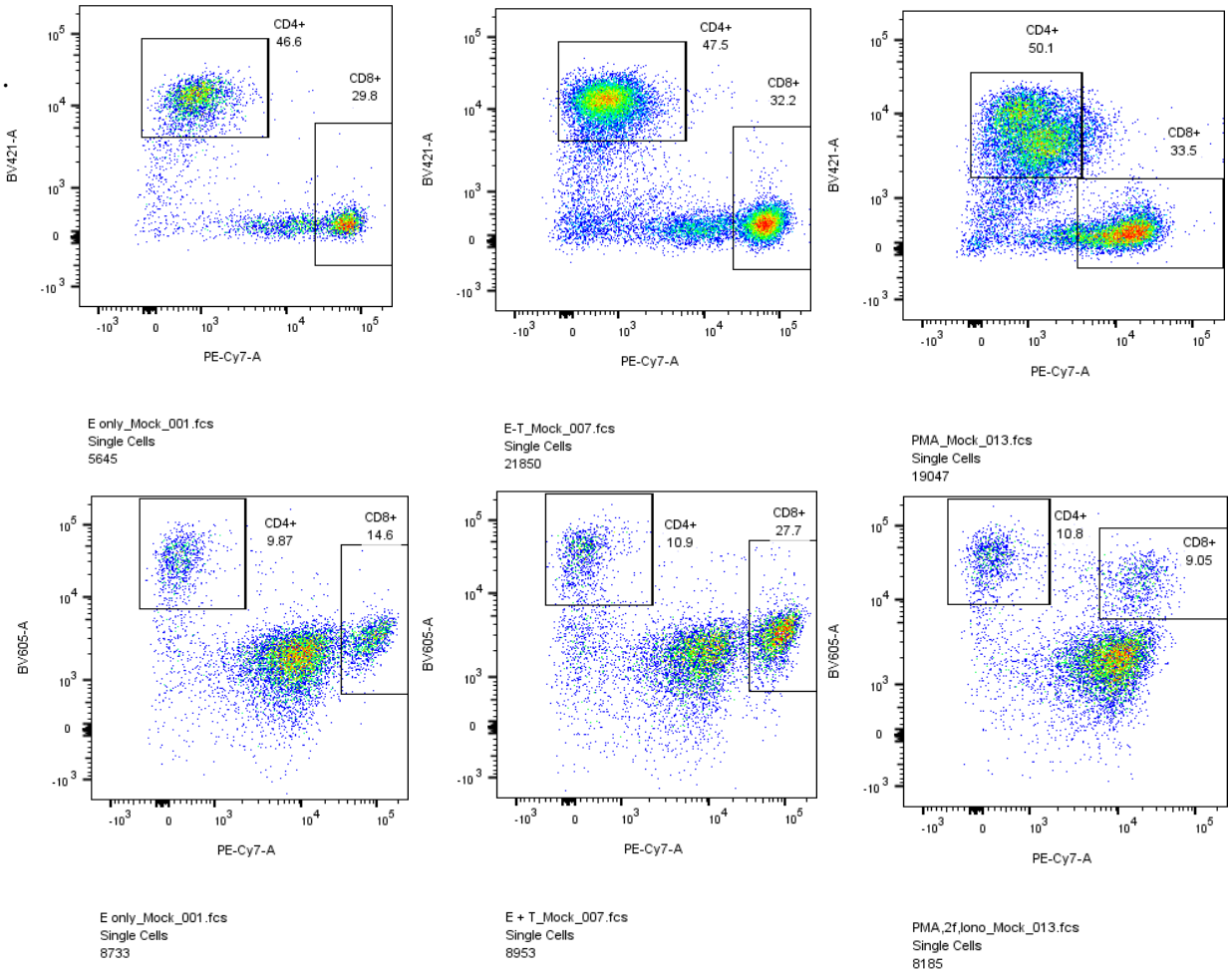

Figure 12a: Gating strategy. Gating strategy of CD4+ and CD8+ T cell subpopulations in cytokine release and degranulation assay. Y-axis: CD4+ marker, x-axis: CD8+ marker.

To compare the level of upregulation of the degranulation marker CD107, and cytokine release profiles between the mCARs and the hCARs in the presence of OSA, a CD107 and cytokine release assay was performed (figure 12b, 12c). As previously mentioned, the humanization of the scFvs was expetced to stabilize the CAR protein, potentially increasing the degranulation

efficacy of the hCARs, as well as enhancing the release of cytolytic factors like Tumor Necrosis Factor (TNF-) α. OSCAR-1^{+} CD4^{+} T cells showed no upregulation of degranulation marker CD107 when co-incubated with OSA, and neither did the CD4^{+} T cells transduced with humanized OS-1 constructs. The CD4^{+} population did show release of TNF-α from OSCAR-1 and the humanized OS-1 constructs, with OSCAR-1 staining 22% positive, and the humanized constructs ranging from 24-37% positive. The CD8^{+} population showed an increase in the degranulation marker CD107 for OSCAR-1 with 21% positive cells, while the humanized constructs ranged from 12-30% positive cells. The CD8+ population showed TNF- α release from 45% of the cells transduced with OSCAR-1, and 40-62% of the cells transduced with the humanized OS-1 constructs.

Figure 12b.

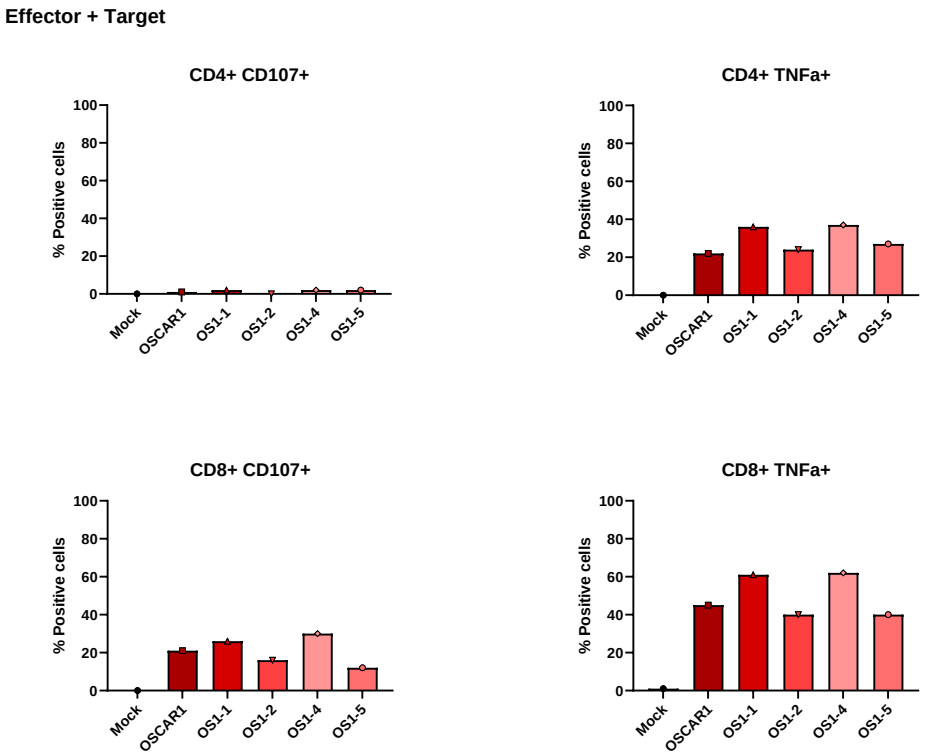

Figure 12b: Cytokine release, OS-1. Murine and humanized OSCAR-1: CD4+/CD8+CD107+ shows CD4+/CD8+ T cells positive for degranulation marker CD107. CD4+/CD8+TNF-α + shows CD4+/CD8+ cells positive for TNF-α release. n=1.

OSCAR-3 $^{+}$CD4^{+} T cells were 8% positive for the degranulation marker CD107, and the CD4^{+} T cells transduced with humanized OS-3 constructs were 13-23% positive for the degranulation

marker. OSCAR-3^{+} CD4^{+} T cells were 12% positive for TNF- α release, and the CD4^{+} T cells transduced with humanized OS-3 constructs were 10-22% positive for TNF- α release. The OSCAR-3^{+} CD8^{+} T cell population were 40% positive for the degranulation marker CD107, while the CD8^{+} T cells transduced with humanized OS-3 constructs ranged from 34-45% positive for CD107. OSCAR-3^{+} CD8^{+} T cells stained 53% positive for TNF- α release, and the CD8+ T cells transduced with humanized OS-3 constructs ranged from 23-45% positive.

Figure 12c.

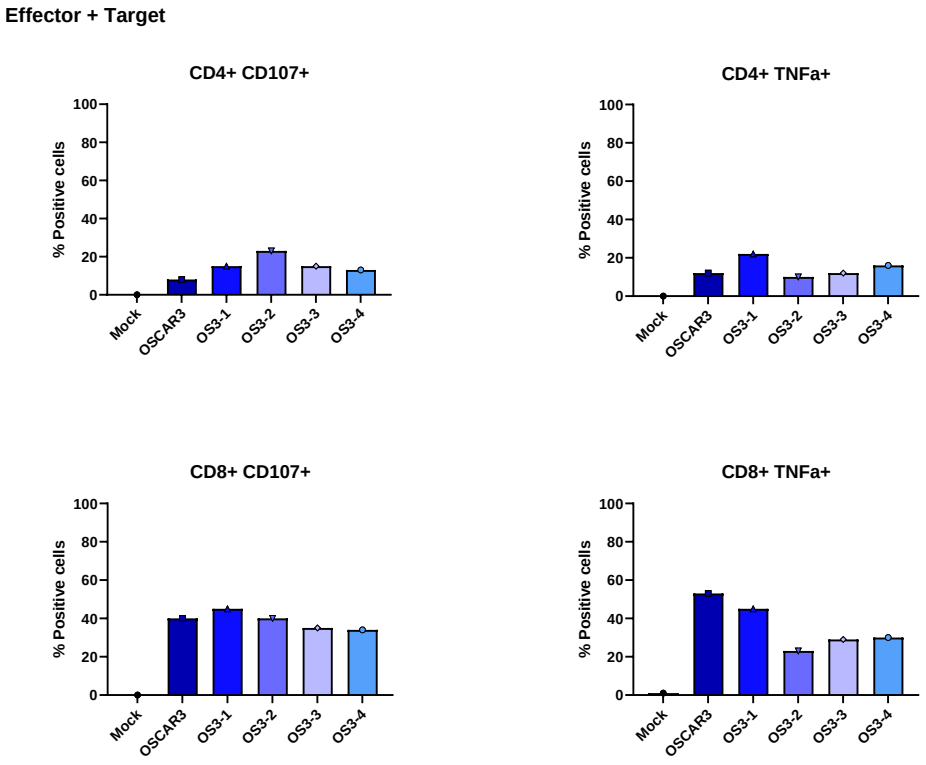

Figure 12c: Cytokine release, OS-3. Murine and humanized OSCAR-3: CD4+/CD8+CD107+ shows CD4+/CD8+ T cells positive for degranulation marker CD107. CD4+/CD8+TNF-α+ shows CD4+/CD8+ cells positive for TNF-α release. n=1.

In conclusion, these results indicate a slight elevation in cytolytic efficacy when comparing the humanized OS1-1 and OS1-4 constructs to OSCAR-1 *in vitro*. Comparing the humanized OS3 constructs to OSCAR-3, the cytolytic efficacy was observed to be either preserved or somewhat lower than the original CAR *in vitro*. Noteably, this experiment needs to be repeated with more donors to have any statistical value.

Comparing cytotoxic persistence between OSCAR-1 and OSCAR-3

To compare the *in vitro* cytotoxic persistance between OSCAR-1 and -3, an exhaustion assay was performed (figure 13). Previous experiments had indicated that OSCAR-1 may be more robust, tolerating repeated stimulation with the target antigen better than OSCAR-3, while maintaining cytotoxic efficiency. If OSCAR-1 had a higher tolerance for exhaustion upon restimulation with the target antigen compared to OSCAR-3, OSCAR-1 was expected to demonstrate superior cytotoxic activity in the final weeks of the exhaustion assay. From the 4 week exhaustion assay performed here, OSCAR-1 and OSCAR-3 performed comparably against OSA. In week 1, OSCAR-1 killed OSA somewhat more efficiently than OSCAR-3, with OSCAR-1 killing 44%, and OSCAR-3 killing 34% after 8 hours, while in week 2 both OSCAR-1 and OSCAR-3 killed approximately 50% of OSA cells. In week 3, after 24 hours, OSCAR-3 killed OSA considerably more efficiently than OSCAR-1, with 94% killing and 67% killing respectively. In week 4, after 24 hours, the killing of OSA was again similar between OSCAR-1 and OSCAR-3, and had declined from 100% killing in week 1, to approximately 84% killing in week 4. Against HEK, after 24 hours, OSCAR-3 was observed to kill somewhat more efficiently compared to OSCAR-1 in the first 2 weeks. OSCAR-3 killed 25% and 35% of HEK cells the first two weeks, and OSCAR-1 killed 10% and 16%. There was no marked difference between OSCAR-3 and OSCAR-1 in week 3 and 4. Against LM7, both OSCAR-1 and OSCAR-3 killed somewhat more efficiently after 8 hours the in the first 2 weeks compared to their killing of OSA at the same time point. In week 1, after 8 hours, OSCAR-1 killed 50% of LM7, and OSCAR-3 killed 60%, while in week 2 OSCAR-1 killed 77%, and OSCAR-3 81%. In week 3, after 24 hours, OSCAR-1 killed only 28% while OSCAR-3 killed 94% of LM7, and in week 4 OSCAR-1 killed approximately 62% while OSCAR-3 killed 85%.

Figure 13.

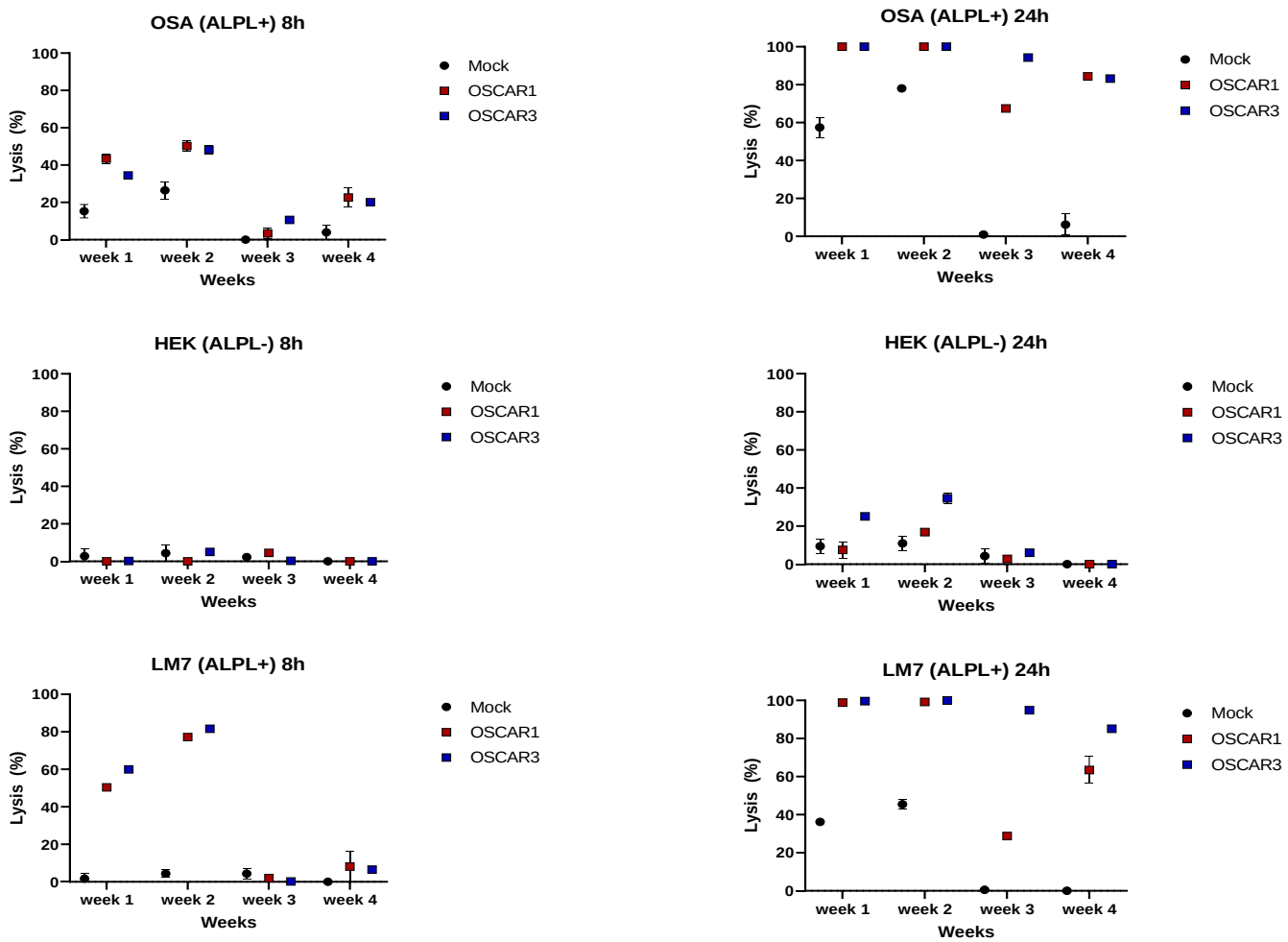

Figure 13: Exhaustion assay (4 weeks rechallenge) of OSCAR-1 and OSCAR-3. n=1.

In conclusion, these result indicate that the cytotoxic persistence is similar between OSCAR-1 and OSCAR-3 *in vitro*. Humanizastion of CARs is expected to increase their stability and cytotoxic persistence, and this experiment should be repeated with the humanized OS-series, and more donors to be statistically significant.

Amino acid sequence alignment of humanized scFvs

Using the Sequence alignment tool in Clone Manager, the murine OSCAR-1 and -3s scFv amino acid sequences were compared to the humanized OS- and OF-series. FRs and CDRs were identified by comparing OSCAR-1 and OSCAR-3 scFv amino acid sequences to that of murine IgG in the Immunogenetics information system (IMGT) database. Substitution mutations were discovered in the FR of the light and heavy chains of the humanized scFvs. No mutations were identified in the CDRs. Further investigation indentified specific mutations suspected to be critical for the function of the scFv. Critical changes were defined based on 2 criteria: 1) the mutation was unique to the non-functional OF-series, and consistent within that series, and 2) the polarity/ charge / branching of the amino acid was significantly changed compared to the canonical amino acid in that specific position. Based on these criteria, 2 critical positions and amino acid substitutions were identified in the OF-1 and OF-3 humanized series (figure 14). In the humanized OF-1 series, the substitution of Aspartic acid with Serine in FR3 of the light chain, and substitution of Glutamic acid with Aspartic acid or Glutamine in FR1 of the heavy chain, were deemed critical. In the humanized OF-3 series, the substitution of Glutamine with Valine at FR1 of the heavy chain, and substitution of Serine with Glycine in FR2 of the heavy chain, were deemed critical.

Figure 14.

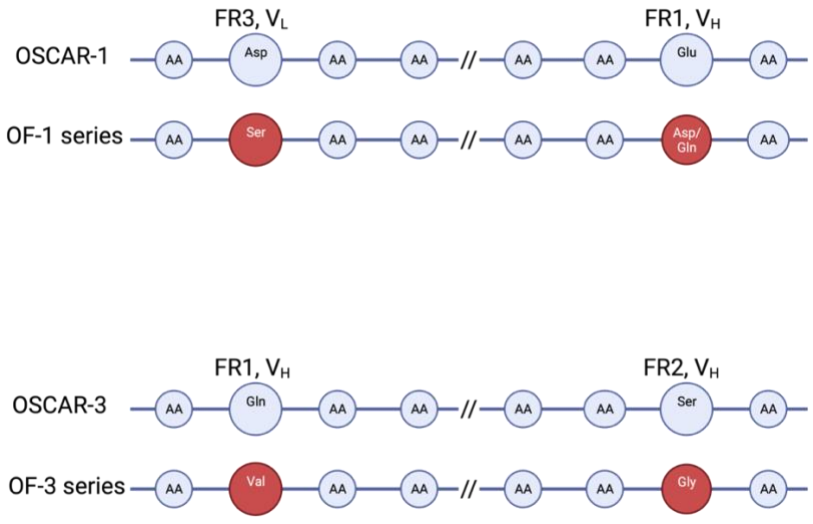

Figure 14: Sequence alignment. Representation of relative position of the 2 assumed critical changes in the amino acid sequences of OF-1 and OF-3 series. Made in Biorender by PA.

Table 9: The table lists the number of substitutions in each framework region of the light and heavy chain of the humanized scFvs, for each construct.

	V_L FR1	V_L FR2	V_L FR3	V_L FR4	V_H FR1	V_H FR2	V_H FR3	V_H FR4
OS1-1	5	1	5	1	2	2	5	2
OS1-2	6	1	5	1	2	2	5	2
OS1-4	6	1	5	1	1	2	6	2
OS1-5	6	1	5	1	1	2	6	2
OS3-1	2	0	8	1	4	3	4	1
OS3-2	2	0	8	1	4	3	4	1
OS3-3	6	0	7	1	4	4	4	1
OS3-4	6	0	7	1	4	3	4	1
OF1-1	7	1	6	0	4	1	9	0
OF1-2	8	3	8	1	4	1	9	0
OF1-3	7	1	6	0	2	2	9	2
OF1-4	8	3	8	1	4	2	9	2
OF3-1	6	1	8	0	2	4	8	0
OF3-3	6	1	8	0	5	6	9	1
OF3-4	7	2	7	3	2	4	9	0
OF3-2	6	1	8	0	5	5	9	1

4. Discussion

The expansion of J76E2 cells transduced with OSCAR-1 and -3, and the humanized OS- and OF-series showed differences between the humanized constructs, but needs to be repeated to have any statistical value. The reduced expansion of constructs of OS3-4, OF1-2, and OF3-1 in J76E2 cells can be a result of the hCAR being inserted within genes essential for proliferation and/or survival, and not necessarily because the constructs themselves reduces viability and growth.

OSCAR-1 was considerably less positive for mFab than OSCAR-3 in J76E2 cells, despite their common murine origin. The humanized OS-1 constructs all showed an increase in mFab recognition, while the humanized OF-1 constructs were all less positive for mFab than OSCAR-1. The humanized OS-3 constructs were less positive for mFab than OSCAR-3, though the range was wide within this series. The humanized OF-3 constructs were consistently and drastically less positive for mFab compared to their murine counterpart. The increase in mFab recognition observed in the OS-1 series was unexpected, because the amino acid sequences of the framework region had been changed to increase similarity with human consensus sequences for V_H and V_L chains. This result may be influenced by the polyclonal anti-mFab used for detection, as we have previsouly observed that batch differences can affect the level of antigen recognition for this antibody. The decrease in mFab recognition observed in the OS-3, OF-1 and OF-3 series was in concord with the humanization of the V_H and V_L chain sequences.

Co-incubation of OSA with J76E2 cells transduced with OSCAR-1 and -3, and the humanized OS constructs showed similar levels of activation between the original mCARs and the hCARs. These results indicate that the OS-series have preserved the ability to recognize and bind OSA, and that the signal transduction through the humanized scFvs has not been disrupted. OS1-4 showed a somewhat elevated activation measured in GMI compared to OSCAR-1, which may indicate a stabilization of the humanized protein. However, it is noteworthy that CAR expression detected by anti-CD34t staining on average was higher for OS1-4 compared to OSCAR-1 and the other OS-1 constructs, and this may have influenced the elevated GMI observed from OS1-4 in the NFAT reporter assays. Moreover, the CD34t expression was in general spread between the humanized constructs of the OS-series and their murine counterpart, making it difficult to directly compare GMI signals from NFAT reporter assays between these constructs. The OF-

series showed no clear activation measured by GMI, and no single cell GFP activation under the microscope. These results may indicate either a disruption in the recognition and binding of the target antigen, a disrupttion of the signal transduction through the scFv, or that the protein is destabilized by humanization and degraded in the cell. No statistically significant difference in EC50 was observed between OSCAR-3 and the humanized OS-3 constructs. These results support that the effective concentration required to reach 50% of the maximum effect has not been altered during the humanization of the OS-3 constructs. However, as previously mentioned the CD34t expression varied noteably between the OS-3 constructs and OSCAR-3. The average CAR expression detected by CD34t was particularly low for construct OS3-2, approximately half of what was detected for OSCAR-3, while the calculated EC50 based on GMI was not significantly different from that of OSCAR-3. Speculation that EC50 between these 2 constructs may have been significantly different if the CD34t expression had been more similar is therefore not unreasonable. It has been demonstrated that EC50 measured in jurkat cells correlates well with EC50 measured in primary T cells[57], therefore these results were expected to translate into subsequent experiments with the humanized OS-3 constructs in PBMCs.

Western blot of J76E2 cells transduced with OSCAR-1 and -3 and the humanized OF-series show that 7 out of 8 humanized CARs from the OF-series were transcribed and translated into protein at a comparable level to the original OSCAR-1 and -3. Furthermore, the intensity of the bands corresponding to the mCARs and hCARs were similar to the bands corresponding to the endogenous CD3ζ, indicating a comparable stability and/ or translational rate among these proteins. The band of hCAR OF1-1 was detected at a higher intensity than OSCAR-1, which could have several causes; the stability of the humanized protein may be increased compared to the murine original, or there may have been an error in counting when preparing the lysate. The experiment should be reapeated with new lysates in order to draw any conclusion regarding the potential increased stability of construct OF1-1.

NFAT reporter assays in IncuCyte and single cell analysis on Flow Cytometry could not detect NFAT-GFP activation of OSCAR-1 in J76E2 cells when co-incubated with OSA. However, NFAT-GFP activated OSCAR-1^{+} cells could be observed in low numbers under the microscope. Previous experiments including both OSCAR-1 and -3 had shown comparable killing efficacy both *in vitro* and *in vivo* between the two OSCARs, so the functionality of OSCAR-1 had already

been demonstrated[45]. OSCAR-1 was for this reason not excluded from further testing in this thesis. These results may indicate that T cell activation through OSCAR-1 engagement induces a different intracellular signalling pathway than through OSCAR-3 engagement, resulting in the nuclear translocation of TFs other than NFAT. Two other canonical pathways downstream of TCR engagement are the NF-κB pathway, and the Mitogen-activated protein kinase (MAPK) pathway, inducing nuclear translocation of TFs NF-κB and AP-1[58], respectively. A triple parameter reporter system in J76 cells has been established, permitting quantification of the activity of NFAT responsive promoters through eGFP, NF-κB responsive promoters through Cyan fluorescent protein (CFP) and AP-1 responsive promoters through mCherry[59], simultaneously. A future experiment employing this reporter system could provide invaluable data elucidating the intracellular signaling pathway downstream of OSCAR-1 engagement.

The incubation of the soluble scFv-IgGs OSCAR-3-IgG, OS3-3-IgG, OF3-4-IgG and OF3-2-IgG with OSA demonstrated that OF3-2 and OF3-4 were not able to recognize and bind the target antigen expressed on OSA. OS3-3 demonstrated a slightly lower level of antigen binding efficacy compared to OSCAR-3, but had retained an effective level of recognition. All of these data taken together prompted the exclusion of the OF-series from further testing in PBMCs.

In PBMCs, a statistically significant difference in expansion was observed between mock and OS1-4, mock and OS1-5 and mock and OS3-3. The reduced expansion may indicate toxicity introduced with the humanized constructs that either affected cell viability, or cytostaticity. In the future, a proliferation assay, for example an Ethynyl-deoxyuridine (EdU) labeling assay[60], could provide useful data regarding the cause of the reduced expansion observed in these constructs.

The level of mFab recognition detected for OS1-1, OS1-2, and OS1-5 in PBMCs was similar or lowered compared to OSCAR-1. Interestingly, OS1-4 transduced PBMCs showed elevated recognition of mFab compared to OSCAR-1, consistent with the result from the staining of the J76E2 cells transduced with OS1-4. These results taken together indicate that OS1-4, despite the "humanization" of the amino acid sequences of the V_H and V_L chains, may have increased immunogenic potential. However, as previously mentioned the result may be influenced by the antibody used for detection, and the experiment should be repeated with a more stably

performing anti-mFab antibody, and more donors. PBMCs transduced with the OS-3 series were all less recognized by mFab compared to OSCAR-3, which is in concord with the humanization of the murine scFv.

After 8 hours killing at E: T ratio 2.5:1, no statistically significant difference was observed between mock, mCARs or hCARs VS. OSA, LM7 or HEK. This is likely because the ratio of effector to target cells was too low to observe any difference between the killing of target positive and negative cell lines at this time point. At 24 hours, mCARs and hCARs were killing OSA and LM7 efficiently at the same ratio. Additionally, there was no difference between mock, mCARs and hCARs VS. HEK at this time point, demonstrating target specificity for both the mCARs and hCARs.

After 8 hours killing at E: T ratio 10:1, a statistically significant difference was observed between mock and mCARs/ hCARs VS. OSA and LM7, but not HEK. This further supports that the killing of OSA and LM7 by $mCAR^+$/ $hCAR^+$ T cells is target specific, and significantly more effective than mock T cells at this time point. After 24 hours at the same ratio, there was observed significant killing of OSA, LM7 and HEK by mCARs and hCARs. This significant killing, or death, of HEK cells under these conditions could be due to a lack of nutrients available caused by competitive $mCAR^+$/ $hCAR^+$ T cells, together with the use of media optimized for T cells. It is likely not caused by TCR specificity, because mock was not observed to kill as efficiently as $mCAR^+$/ $hCAR^+$ T cells. OSCAR-1 and -3 have previously exhibited tonic signaling, resulting in unspecific release of perforin and granzyme B to varying degrees. Tonic signaling may increase the cell metabolism, and the CAR^+ T cells may therefore require more nutrients compared to mock T cells. Concomitantly, the tonic release, or "leaking", of perforin and proinflammatory cytokines[61] from the $mCAR^+$/ $hCAR^+$ T cells would negatively affect the HEK cells viability. Tonicity could therefore help explain the increased killing of target negative HEK cells by $mCAR^+$/ $hCAR^+$ T cells, and the lack of comparable killing by mock T cells. The most probable cause for the unspecific killing of HEK is a combination of tonic activity from $mCAR^+$/ $hCAR^+$ T cells, and competition for nutrients in an environment favoring T cells over cancer cells.

Based on the average killing % of OSA at the lowest ratio where the difference between mock and mCAR is statistically significant, the difference between OSCAR-1 and OS1-4, and

OSCAR-3 and OS3-1 is the lowest. This means that based on this experiment, OS1-4 has retained most of OSCAR-1s killing capacity, and OS3-1 has retained most of OSCAR-3s killing capacity, out of the 8 humanized constructs from the OS-series.

The gating of $CD4^+$ and $CD8^+$ subpopulations of the degranulation and cytokine release assay showed a shift in the $CD8^+$ T cell scattering when induced with PMA/ Ionomycin. The $CD8^+$ population shifted up along the Y-axis, appearing to be $CD4^+CD8^+$ double positive cells. After consulting with our labs Flow Cytometry expert, the gated population shown in figure 12a was determined to be the true $CD8^+$ subpopulation. Noteably, the viability of the cells used for this assay was low, with viability after thawing ranging from 45-73% and 32-62% for OSCAR-1/OS-1 and OSCAR-3/ OS-3 respectively. The high number of cells in total (dying + alive) may have affected the results of the experiments, due to elevated waste and cytoplasmic metabolites. The low viability is also an indication that the live cells were in poor condition, and for this reason could not be activated to their full potential.

The OSCAR-1^+CD4^+ population was negative for CD107 in this experiment, as was the OS-1 series transduced $CD4^+$ cells. Unpublished data from our lab has previously shown $CD107^+$ of around 20% for OSCAR-1^+CD4^+ cells co-incubated with OSA. OSCAR-1, OS1-2 and OS1-5 showed comparable release of TNF-α in $CD4^+$ cells, while OS1-1 and OS1-4 showed a slight increase in TNF-α release. The OSCAR-1^+CD8^+ population was positive for CD107, OS1-2 and OS1-5 $CD8^+$ T cells showed a slight decrease in $CD107^+$ cells, while OS1-1 and OS1-4 $CD8^+$ T cells showed a slight increase compared to OSCAR-1. Similarly, for the $CD8^+$ population, OS1-1 and OS1-4 showed an increase in TNF-α release compared to OSCAR-1, and OS1-2 and OS1-5 showed decreased TNF-α release.

The OSCAR-3^+CD4^+ population showed upregulation of CD107 compared to mock, while all the humanized OS-3 constructs showed a slight increase in CD107 upregulation compared to OSCAR-3. The $CD4^+$ population showed upregulation of TNF-α release in OSCAR-3, OS3-2, OS3-3 and OS3-4 compared to mock, while OS3-1 showed a slight increase in TNF-α release compared to OSCAR-3. The $CD8^+$ population showed very similar expression of CD107 marker in OSCAR-3 and OS3-2, while a slight increase was observed in OS3-1, and a slight decrease was observed in OS3-3 and OS3-4. For TNF-α release, OS3-1 $CD8^+$ T cells were slightly less positive than OSCAR-3 $CD8^+$ T cells, and OS-2, OS3-3 and OS3-4 $CD8^+$ T cells were

considerably less positive for TNF-α release compared to OSCAR-3. Because the experiment only used 1 donor, no conclusion can be drawn from these results. The degranulation and cytokine release assay should be repeated with cells of a higher viability, and with more donors to be statistically relevant. Interestingly, in 2021 it was demonstrated that the amino acid composition of FRs in scFvs derived from murine antibodies have direct effects on CAR tonic signaling, and may be corrected with amino acid substitution during humanization[62]. In the future, it may therefore be of interest to compare the tonicity of the mCARs and hCARs as well.

In the exhaustion assay, OSCAR-1 and OSCAR-3 overall performed quite similar. OSCAR-3 killed more efficiently than OSCAR-1 in week 3, against both OSA and LM7, but OSCAR-1 recovered and killed efficiently again in week 4. The elevated lysis of HEK by OSCAR-3 observed in week 1 and 2 is likely due to tonicity, as we have previously observed a higher level of tonic signaling in OSCAR-3 compared to OSCAR-1. The use of LM7 as feeder cells could have affected the stimulation of OSCAR-1 and -3, as we have previously observed that the choice of feeder cells can influences the rate of their exhaustion (unpublished data). The exhaustion assay should be repeated with the inclusion of the humanized OS-series to evaluate whether the humanization altered the functional persistance of the CAR, and with more donors to be statistically relevant.

The results of expansion, expression and killing of OSA with PBMCs transduced with the humanized OS-3 series taken together, the humanized candidate most similar to OSCAR-3 is OS3-1. The difference in expansion between mock, OSCAR-3 and OS3-1 was not statistically significant, the recognition of mFab had been reduced compared to OSCAR-3, and the difference in the average killing % of OSA was the lowest between OS3-1 and OSCAR-3 at both 10:1, 8 hours, and 2.5:1, 24 hours. The most similar humanized candidate to OSCAR-1 was less obvious, but based on the killing of OSA with PBMCs transduced with the OS-1 series, the candidate that retained most of OSCAR-1s killing efficacy overall was OS1-4. However, OS1-4 showed a significantly increased recognition of mFab compared to OSCAR-1, and the difference in expansion between mock and OS1-4 was statistically significant. Evaluating other candidates from the OS-1 series based on killing, OS1-1 and OS1-2 stood out. At 10:1, 8 hours, the second most similar candidate to OSCAR-1 was OS1-1, and at 2.5:1, 24 hours, the most similar candidate to OSCAR-1 was OS1-2. The recognition of mFab was similar between OS1-1 and

OSCAR-1, but had decreased for OS1-2. There was no statistically significant difference in expansion between mock and OS1-1, or mock and OS1-2. These data taken together suggested that OS1-2 could be a decent humanized candidate when assessing similarity.

Sequence alignment of the murine and humanized scFv amino acid sequences uncovered that all mutations were substitutions located within the FRs of the scFv; The CDRs were not modified. Substitutions in the FRs may induce alterations in the folding of the protein, and the funtional characteristics of the CAR. Particularly, mutations in the FR1 of the scFv heavy chain can have dramatic effects on target affinity, even in the absence of major conformational changes[63]. Key amino acids in the FRs of heavy and light chains, named Vernier zone residues, influence correct CDR loop orientation, and are often back-mutated during humanization of antibodies[64] in order to preserve antigen binding affinity. One particularly well recognized Vernier zone residue is found in position 71 of the heavy chain[65,64], and the importance of preserving the original amino acid in this position was demonstrated during humanization of the murine antibodies anti-lyzosome mAb D1.3[66], anti-acetylcholine receptor mAb 198[67], and anti-tumor-associated glycoprotein mAb B72.3[68]. Yet, there are examples of amino acid substitution in this position that are well tolerated during antibody humanization[69].

Detailed analysis led to the discovery of 2 assumed critical changes both in the humanized OSCAR-1s and humanized OSCAR-3s. Between OSCAR-1 and the humanized OF-1 series, the substitution of Aspartic acid with Serine in FR3 of the scFv light chain was deemed critical. Aspartic acid was a negatively charged amino acid with a carboxyl group in the side chain, which was replaced by a polar uncharged Serine, resulting in a net change in charge in this specific position. The charge and polarity of the amino acid determines whether it attracts or repels sequential or spatial neighboring amino acids, and may affect protein folding. The second substitution in this series deemed critical was the switch from Glutamic acid to Aspartic acid or Glutamine in FR1 of the scFv heavy chain. OF1-1 and OF1-2 contained the substitution of Aspartic acid, and OF1-3 and OF1-4 contained the substitution of Glutamine. Aspartic acid and Glutamic acid were both negatively charged under physiological conditions, but the side chain of Aspartic acid was less branched. Difference in branching, despite maintaining net negative charge in this position of the heavy chain FR1, may affect secondary protein structure and antigen affinity, as previously stated. Glutamine was polar, but uncharged, leading to a net

change in charge in this position. Between OSCAR-3 and the humanized OF-3 series, the substitution of Glutamine in FR1 of the scFv heavy chain with Valine was deemed critical. Glutamine was polar uncharged, and replaced with a hydrophobic Valine. Although the differences in branching between the two amino acids seemed significant, the main reason this substitution was deemed critical was it´s position within heavy chain FR1, and the switch from a polar (hydrophilic) amino acid to a hydrophobic one. The second substitution deemed critical in this series was the switch from Serine to Glycine in FR2 of the scFv heavy chain. Serine was a polar uncharged amino acid with a branching side chain while Glycine lacked a side chain, effectively rendering it non-polar.

Substitutions of Vernier zone residue 71 of the heavy chain (V71) was only identified in constructs OF1-1 and OF1-2. Because only 2 out of 8 constructs that demonstrated loss of target recognition and binding contained a substitution in the V71, this substitution could not be the sole cause of loss of reactivity. Since no mutations were identitfied in the CDRs of the humanized scFvs, the lack of reactivity observed in the OF-series is likely not due to mismatch of amino acids in the epitope-paratope interface. The lack of reactivity is more likely caused by alterations in the spatial arrangement of the amino acids of the CDR loops, stemming from mutations in the FRs (illustration 12), or reduced target affinity caused by amino acid substitutions in the FR1 of the heavy chain.

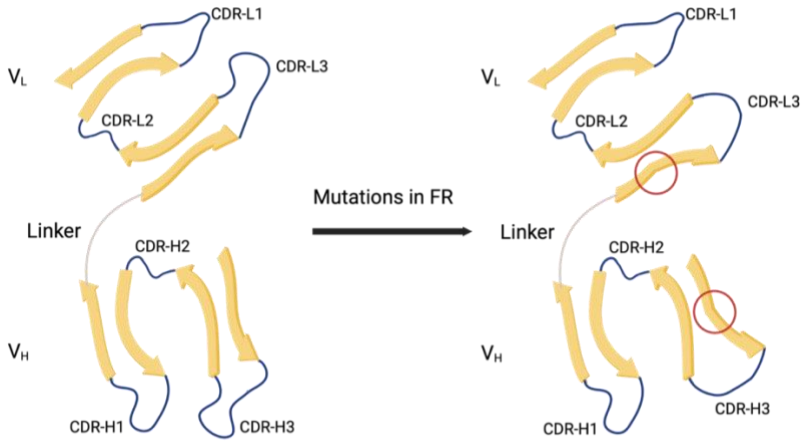

Illustration 12: scFv conformation. The illustration shows how mutations in FRs (red circle) may disrupt the spatial arrangement of the CDR loops.

In illustration 12, the FRs (yellow arrows) are mutated (red circle), resulting in disruption of their native protein structure, and the subsequent spatial re-arrangement the of the up- and downstream CDR loops.

In summary, the results of these experiments taken together indicate that 8 of the 16 humanized constructs, the OS-series, may be good candidates for further *in vitro* and *in vivo* testing, particularly constructs OS1-2 and OS3-1. While the *in vitro* experiments described here indicate that some humanized constructs have retained the cytotoxic functions of their murine counterpart, such as OS1-4 and OS3-1, the humanization did not consistently reduce the immunogenic potential of the scFvs as demonstrated by the elevated mFab recognition of OS1-4. However, the consistently increased mFab recognition after humanization of construct OS1-4 may not necessarily translate to increased immunigenicity *in vivo*, and further testing of this construct could provide useful data, further elucidating the many nuances encompassed in the term “humanization”.

Bibliografy

1. Ottaviani, G. & Jaffe, N. The Epidemiology of Osteosarcoma. in *Pediatric and Adolescent Osteosarcoma* (eds. Jaffe, N., Bruland, O. S. & Bielack, S.) 3–13 (Springer US, 2010). doi:10.1007/978-1-4419-0284-9_1.
2. Cole, S., Gianferante, D. M., Zhu, B. & Mirabello, L. Osteosarcoma: A Surveillance, Epidemiology, and End Results program-based analysis from 1975 to 2017. *Cancer* **128**, 2107–2118 (2022).
3. Mirabello, L., Troisi, R. J. & Savage, S. A. International osteosarcoma incidence patterns in children and adolescents, middle ages and elderly persons. *Int. J. Cancer* **125**, 229–234 (2009).
4. Odri, G. A., Tchicaya-Bouanga, J., Yoon, D. J. Y. & Modrowski, D. Metastatic Progression of Osteosarcomas: A Review of Current Knowledge of Environmental versus Oncogenic Drivers. *Cancers* **14**, 360 (2022).
5. Prater, S. & McKeon, B. Osteosarcoma. in *StatPearls* (StatPearls Publishing, 2023).
6. Misaghi, A., Goldin, A., Awad, M. & Kulidjian, A. A. Osteosarcoma: a comprehensive review. *SICOT-J* **4**, 12 (2018).
7. Isakoff, M. S., Bielack, S. S., Meltzer, P. & Gorlick, R. Osteosarcoma: Current Treatment and a Collaborative Pathway to Success. *J. Clin. Oncol.* **33**, 3029–3035 (2015).
8. Casali, P. G. *et al.* Bone sarcomas: ESMO–PaedCan–EURACAN Clinical Practice Guidelines for diagnosis, treatment and follow-up††FootnotesApproved by the ESMO Guidelines Committee, PaedCan and EURACAN: August 2018. *Ann. Oncol.* **29**, iv79–iv95 (2018).

9. van den Boogaard, W. M. C., Komninos, D. S. J. & Vermeij, W. P. Chemotherapy Side-Effects: Not All DNA Damage Is Equal. *Cancers* **14**, 627 (2022).
10. Yahiro, K. & Matsumoto, Y. Immunotherapy for osteosarcoma. *Hum. Vaccines Immunother.* **17**, 1294–1295 (2021).
11. Boye, K. *et al.* Pembrolizumab in advanced osteosarcoma: results of a single-arm, open-label, phase 2 trial. *Cancer Immunol. Immunother.* **70**, 2617–2624 (2021).
12. Zhang, Z., Tan, X., Jiang, Z., Wang, H. & Yuan, H. Immune checkpoint inhibitors in osteosarcoma: A hopeful and challenging future. *Front. Pharmacol.* **13**, 1031527 (2022).
13. Han, G., Bi, W.-Z., Xu, M., Jia, J.-P. & Wang, Y. Amputation Versus Limb-Salvage Surgery in Patients with Osteosarcoma: A Meta-analysis. *World J. Surg.* **40**, 2016–2027 (2016).
14. Harris, J. D., Trinh, T. Q., Scharschmidt, T. J. & Mayerson, J. L. Exceptional functional recovery and return to high-impact sports after Van Nes rotationplasty. *Orthopedics* **36**, e126-131 (2013).
15. Hameed, M. & Mandelker, D. Tumor Syndromes Predisposing to Osteosarcoma. *Adv. Anat. Pathol.* **25**, 217–222 (2018).
16. Zhou, B. *et al.* Notch signaling pathway: architecture, disease, and therapeutics. *Signal Transduct. Target. Ther.* **7**, 1–33 (2022).
17. FOS Fos proto-oncogene, AP-1 transcription factor subunit [Homo sapiens (human)] - Gene - NCBI. https://www.ncbi.nlm.nih.gov/gene/2353.
18. Czarnecka, A. M. *et al.* Molecular Biology of Osteosarcoma. *Cancers* **12**, 2130 (2020).
19. Veselska, R. *et al.* Nestin expression in osteosarcomas and derivation of nestin/CD133 positive osteosarcoma cell lines. *BMC Cancer* **8**, 300 (2008).

20. Brown, H. K., Tellez-Gabriel, M. & Heymann, D. Cancer stem cells in osteosarcoma. *Cancer Lett.* **386**, 189–195 (2017).
21. Krazz, M. THE CELL Molecular Biology of Sixth Edition.
22. Dunn, G. P., Old, L. J. & Schreiber, R. D. The Three Es of Cancer Immunoediting. *Annu. Rev. Immunol.* **22**, 329–360 (2004).
23. Tokarew, N., Ogonek, J., Endres, S., von Bergwelt-Baildon, M. & Kobold, S. Teaching an old dog new tricks: next-generation CAR T cells. *Br. J. Cancer* **120**, 26–37 (2019).
24. Del Bufalo, F. *et al.* GD2-CART01 for Relapsed or Refractory High-Risk Neuroblastoma. *N. Engl. J. Med.* **388**, 1284–1295 (2023).
25. Liu, G., Rui, W., Zhao, X. & Lin, X. Enhancing CAR-T cell efficacy in solid tumors by targeting the tumor microenvironment. *Cell. Mol. Immunol.* **18**, 1085–1095 (2021).
26. Rajani, C. *et al.* 7 - Cancer-targeted chemotherapy: Emerging role of the folate anchored dendrimer as drug delivery nanocarrier. in *Pharmaceutical Applications of Dendrimers* (eds. Chauhan, A. & Kulhari, H.) 151–198 (Elsevier, 2020). doi:10.1016/B978-0-12-814527-2.00007-X.
27. Foeng, J., Comerford, I. & McColl, S. R. Harnessing the chemokine system to home CAR-T cells into solid tumors. *Cell Rep. Med.* **3**, 100543 (2022).
28. Bommhardt, U., Schraven, B. & Simeoni, L. Beyond TCR Signaling: Emerging Functions of Lck in Cancer and Immunotherapy. *Int. J. Mol. Sci.* **20**, 3500 (2019).
29. Figure 1. Comparison between T cell receptor (TCR) and chimeric antigen... *ResearchGate* https://www.researchgate.net/figure/Comparison-between-T-cell-receptor-TCR-and-chimeric-antigen-receptor-CAR-structure_fig1_340032999.

30. Macian, F. NFAT proteins: key regulators of T-cell development and function. *Nat. Rev. Immunol.* **5**, 472–484 (2005).
31. Shah, K., Al-Haidari, A., Sun, J. & Kazi, J. U. T cell receptor (TCR) signaling in health and disease. *Signal Transduct. Target. Ther.* **6**, 1–26 (2021).
32. McKean, M. & Amaria, R. Using Adoptive Cell Therapy in the Modern Era of Metastatic Melanoma Treatment. *Clin. Skin Cancer* **2**, 32–38 (2017).
33. Kumar, A., Watkins, R. & Vilgelm, A. E. Cell Therapy With TILs: Training and Taming T Cells to Fight Cancer. *Front. Immunol.* **12**, (2021).
34. Cornel, A. M., Mimpen, I. L. & Nierkens, S. MHC Class I Downregulation in Cancer: Underlying Mechanisms and Potential Targets for Cancer Immunotherapy. *Cancers* **12**, 1760 (2020).
35. Srivastava, A. K., Guadagnin, G., Cappello, P. & Novelli, F. Post-Translational Modifications in Tumor-Associated Antigens as a Platform for Novel Immuno-Oncology Therapies. *Cancers* **15**, 138 (2022).
36. King, D. *Chimeric Antigen Receptor (CAR) T-Cell Therapy*. (2020).
37. Arasanz, H. *et al.* PD1 signal transduction pathways in T cells. *Oncotarget* **8**, 51936–51945 (2017).
38. Guntermann, C. & Alexander, D. R. CTLA-4 suppresses proximal TCR signaling in resting human CD4(+) T cells by inhibiting ZAP-70 Tyr(319) phosphorylation: a potential role for tyrosine phosphatases. *J. Immunol. Baltim. Md 1950* **168**, 4420–4429 (2002).
39. Lee, H. T., Lee, S. H. & Heo, Y.-S. Molecular Interactions of Antibody Drugs Targeting PD-1, PD-L1, and CTLA-4 in Immuno-Oncology. *Molecules* **24**, 1190 (2019).
40. Allison, J. P. Immune Checkpoint Blockade in Cancer Therapy.

41. Honjo, T. Serendipities of Acquired Immunity. *TRENDS Sci.* **24**, 9_80-9_97 (2019).
42. Carlino, M. S., Larkin, J. & Long, G. V. Immune checkpoint inhibitors in melanoma. *The Lancet* **398**, 1002–1014 (2021).
43. Walsh, R. J., Sundar, R. & Lim, J. S. J. Immune checkpoint inhibitor combinations—current and emerging strategies. *Br. J. Cancer* **128**, 1415–1417 (2023).
44. Bruland, Ø., Fodstad, Ø., Funderud, S. & Pihl, A. New monoclonal antibodies specific for human sarcomas. *Int. J. Cancer* **38**, 27–31 (1986).
45. Mensali, N. *et al.* ALPL-1 is a target for chimeric antigen receptor therapy in osteosarcoma. *Nat. Commun.* **14**, 3375 (2023).
46. Gorovits, B. & Koren, E. Immunogenicity of Chimeric Antigen Receptor T-Cell Therapeutics. *BioDrugs Clin. Immunother. Biopharm. Gene Ther.* **33**, 275–284 (2019).
47. Maetzig, T., Galla, M., Baum, C. & Schambach, A. Gammaretroviral Vectors: Biology, Technology and Application. *Viruses* **3**, 677–713 (2011).
48. Maus, M. V. *et al.* T Cells Expressing Chimeric Antigen Receptors Can Cause Anaphylaxis in Humans. *Cancer Immunol. Res.* **1**, 26–31 (2013).
49. Khan, A. N. *et al.* Immunogenicity of CAR-T Cell Therapeutics: Evidence, Mechanism and Mitigation. *Front. Immunol.* **13**, 886546 (2022).
50. Kim, J. H. & Hong, H. J. Humanization by CDR grafting and specificity-determining residue grafting. *Methods Mol. Biol. Clifton NJ* **907**, 237–245 (2012).
51. Myers, R. M. *et al.* Humanized CD19-Targeted Chimeric Antigen Receptor (CAR) T Cells in CAR-Naive and CAR-Exposed Children and Young Adults With Relapsed or Refractory Acute Lymphoblastic Leukemia. *J. Clin. Oncol.* **39**, 3044–3055 (2021).

52. Gauthier, J. *et al.* Factors associated with outcomes after a second CD19-targeted CAR T-cell infusion for refractory B-cell malignancies. *Blood* **137**, 323–335 (2021).
53. Huang, L. *et al.* Safety and Efficacy of Humanized Versus Murinized CD19 and CD22 CAR T-Cell Cocktail Therapy for Refractory/Relapsed B-Cell Lymphoma. *Cells* **11**, 4085 (2022).
54. Ishikawa, A. *et al.* Improved anti-solid tumor response by humanized anti-podoplanin chimeric antigen receptor transduced human cytotoxic T cells in an animal model. *Genes Cells* **27**, 549–558 (2022).
55. Ohtsuka, T., Kaziro, Y. & Satoh, T. Analysis of the T-cell activation signaling pathway mediated by tyrosine kinases, protein kinase C, and Ras protein, which is modulated by intracellular cyclic AMP. *Biochim. Biophys. Acta BBA - Mol. Cell Res.* **1310**, 223–232 (1996).
56. Chatila, T., Silverman, L., Miller, R. & Geha, R. Mechanisms of T cell activation by the calcium ionophore ionomycin. *J. Immunol. Baltim. Md 1950* **143**, 1283–1289 (1989).
57. Wang, X. *et al.* Extensive functional comparisons between chimeric antigen receptors and T cell receptors highlight fundamental similarities. *Mol. Immunol.* **138**, 137–149 (2021).
58. Conley, J. M., Gallagher, M. P. & Berg, L. J. T Cells and Gene Regulation: The Switching On and Turning Up of Genes after T Cell Receptor Stimulation in CD8 T Cells. *Front. Immunol.* **7**, (2016).
59. Rosskopf, S. *et al.* A Jurkat 76 based triple parameter reporter system to evaluate TCR functions and adoptive T cell strategies. *Oncotarget* **9**, 17608–17619 (2018).
60. Flomerfelt, F. A. & Gress, R. E. Analysis of Cell Proliferation and Homeostasis Using EdU Labeling. *Methods Mol. Biol. Clifton NJ* **1323**, 211–220 (2016).

61. Chen, J. *et al.* Tuning charge density of chimeric antigen receptor optimizes tonic signaling and CAR-T cell fitness. *Cell Res.* **33**, 341–354 (2023).
62. Landoni, E. *et al.* Modifications to the Framework Regions Eliminate Chimeric Antigen Receptor Tonic Signaling. *Cancer Immunol. Res.* **9**, 441–453 (2021).
63. The VH framework region 1 as a target of efficient mutagenesis for generating a variety of affinity-matured scFv mutants | Scientific Reports. https://www.nature.com/articles/s41598-021-87501-7.
64. Antibodies | Free Full-Text | Antibody Structure and Function: The Basis for Engineering Therapeutics. https://www.mdpi.com/2073-4468/8/4/55.
65. Fernández-Quintero, M. L., Kroell, K. B., Hofer, F., Riccabona, J. R. & Liedl, K. R. Mutation of Framework Residue H71 Results in Different Antibody Paratope States in Solution. *Front. Immunol.* **12**, (2021).
66. Verhoeyen, M., Milstein, C. & Winter, G. Reshaping Human Antibodies: Grafting an Antilysozyme Activity. *Science* **239**, 1534–1536 (1988).
67. Papanastasiou, D. *et al.* Construction and characterization of a humanized single chain Fv antibody fragment against the main immunogenic region of the acetylcholine receptor. *J. Neuroimmunol.* **94**, 182–195 (1999).
68. Xiang, J., Sha, Y., Jia, Z., Prasad, L. & Delbaere, L. T. J. Framework Residues 71 and 93 of the Chimeric B72.3 Antibody are Major Determinants of the Conformation of Heavy-chain Hypervariable Loops. *J. Mol. Biol.* **253**, 385–390 (1995).
69. Teplyakov, A. *et al.* Structural insights into humanization of anti-tissue factor antibody 10H10. *mAbs* **10**, 269–277 (2018).